Eur. Phys. J. B **62**, 129–145 (2008)
DOI: 10.1140/epjb/e2008-00138-5

THE EUROPEAN PHYSICAL JOURNAL B

A local moment approach to the gapped Anderson model

M.R. Galpin[a] and D.E. Logan

Physical and Theoretical Chemistry Laboratory, Oxford University, South Parks Road, Oxford, OX1 3QZ, UK

Received 31 January 2008 / Received in final form 1st March 2008
Published online 4 April 2008 –

Abstract. We develop a non-perturbative local moment approach (LMA) for the gapped Anderson impurity model (GAIM), in which a locally correlated orbital is coupled to a host with a gapped density of states. Two distinct phases arise, separated by a level-crossing quantum phase transition: a screened singlet phase, adiabatically connected to the non-interacting limit and as such a generalized Fermi liquid (GFL); and an incompletely screened, doubly degenerate local moment (LM) phase. On opening a gap (δ) in the host, the transition occurs at a critical gap δ_c, the GFL [LM] phase occurring for $\delta < \delta_c$ [$\delta > \delta_c$]. In agreement with numerical renormalization group (NRG) calculations, the critical $\delta_c = 0$ at the particle-hole symmetric point of the model, where the LM phase arises immediately on opening the gap. In the generic case by contrast $\delta_c > 0$, and the resultant LMA phase boundary is in good quantitative agreement with NRG results. Local single-particle dynamics are considered in some detail. The major difference between the two phases resides in bound states within the gap: the GFL phase is found to be characterised by one bound state only, while the LM phase contains two such states straddling the chemical potential. Particular emphasis is naturally given to the strongly correlated, Kondo regime of the model. Here, single-particle dynamics for both phases are found to exhibit universal scaling as a function of scaled frequency ω/ω_m^0 for fixed gaps δ/ω_m^0, where ω_m^0 is the characteristic Kondo scale for the gapless (metallic) AIM; at particle-hole symmetry in particular, the scaling spectra are obtained in closed form. For frequencies $|\omega|/\omega_m^0 \gg \delta/\omega_m^0$, the scaling spectra are found generally to reduce to those of the gapless, metallic Anderson model; such that for small gaps $\delta/\omega_m^0 \ll 1$ in particular, the Kondo resonance that is the spectral hallmark of the usual metallic Anderson model persists more or less in its entirety in the GAIM.

PACS. 72.15.Qm Scattering mechanisms and Kondo effect – 75.20.Hr Local moment in compounds and alloys; Kondo effect, valence fluctuations, heavy fermions

1 Introduction

The Anderson impurity model (AIM) [1] plays a central role in our understanding of correlated physics in many-electron systems. Comprising a single impurity site with local Coulomb interaction, coupled to a a non-interacting band of metallic electrons, it describes a range of interesting physical phenomena—most notably the celebrated Kondo effect in dilute metal alloys [2] and mesoscopic quantum dots [3].

The spin-$\frac{1}{2}$ Kondo effect arising in the AIM is now well understood by a combination of exact and approximate theoretical approaches [2]. Below some characteristic Kondo temperature T_K, a complex many-body state develops in which the impurity spin is completely screened by the host metal, leading at low energies to a 'local' Fermi liquid.

Here by contrast we consider an Anderson impurity in a *gapped* host, where the density of states vanishes over a finite range about the chemical potential; a model of relevance to Anderson impurities in both semiconductors and BCS superconductors [4–7] (the latter in the particle-hole symmetric limit mapping on to a particular gapped AIM, see *e.g.* [5]). Since the Kondo effect in metals relies on the existence of conduction band states near the Fermi level [2], the gapped AIM (GAIM) naturally displays rather different physics from its metallic analogue.

Indeed, aspects of its rich behaviour have been discussed in the literature. Early studies involved approximate analytical methods (poor man's scaling, $1/N$ and non-crossing expansions) [8,9], quantum Monte Carlo [8–10] and the numerical renormalization group (NRG) [10]. At a critical value of the gap, δ_c, each predicted a quantum phase transition, between a Kondo-screened phase and a 'local moment' (LM) phase where the impurity spin remains free as $T \to 0$, but no general consensus was reached as to the nature and location of the transition. The NRG was later used to calculate thermodynamics of the model by Chen and Jayaprakash [11], who also derived an effective low-energy Hamiltonian

[a] e-mail: mrg@physchem.ox.ac.uk

showing that a level-crossing transition from singlet to doublet ground-states arises above δ_c, with δ_c identically zero when the model is particle-hole symmetric. A density-matrix renormalization-group approach [12], on the other hand, found no qualitative difference between the particle-hole symmetric and asymmetric cases. The present authors have confirmed [13] that the NRG picture [11] is correct by considering perturbation theory to all orders in the Coulomb interaction, U; showing that the singlet phase behaves as a generalized Fermi liquid (GFL) in the sense of being perturbatively connected to the non-interacting limit, but that the particle-hole symmetric point of the model is not perturbatively connected to the non-interacting limit for any non-zero gap, and as such is a non-Fermi liquid.

In this work we analyze the GAIM using the local moment approach (LMA) [14–17], which has hitherto been used successfully to describe the metallic Anderson model itself [14–16], the pseudogap Anderson model [17–20], and the periodic Anderson model within dynamical mean-field theory [21–23]. Here we extend the approach to encompass the subtle physics of the GAIM. By comparison to results from NRG [11] we show that the LMA indeed captures the problem rather well, recovering for example the exact asymptotic behaviour of bound states in the gap, and yielding very good agreement with NRG results for the phase diagram of the model. New results for single-particle dynamics of the GAIM on all energy scales are also obtained, including in particular universal scaling behaviour in the strong coupling, Kondo regime of the model.

The structure of the paper is as follows. We begin by outlining the relevant background material in Section 2, before moving on to a more detailed discussion and analysis of the NRG results [11] in Section 3. Our implementation of the LMA for the GAIM is given in Section 4, and in Sections 5 and 6 our analytical and numerical results are presented. The paper ends with a conclusion.

2 The gapped Anderson model

In conventional notation we write the generic Anderson Hamiltonian [2] as

$$\hat{H} = \sum_{\mathbf{k},\sigma} \epsilon_{\mathbf{k}} \hat{n}_{\mathbf{k}\sigma} + \sum_{\sigma} \epsilon_{\mathrm{i}} \hat{n}_{\mathrm{i}\sigma} + U \hat{n}_{\mathrm{i}\uparrow} \hat{n}_{\mathrm{i}\downarrow} + \sum_{\mathbf{k},\sigma} (V_{\mathbf{ik}} c^{\dagger}_{\mathbf{k}\sigma} c_{\mathrm{i}\sigma} + \mathrm{h.c.}) \tag{1}$$

where $\hat{n}_{j\sigma} = c^{\dagger}_{j\sigma} c_{j\sigma}$ is the number operator for σ-spin electrons on site j (with $j = \mathrm{i}$ referring to the impurity site and $j \equiv \mathbf{k}$ to the host band states). The first term in equation (1) thus describes the non-interacting host band, the second and third terms describe the impurity with onsite interaction U, and the fourth term hybridizes the two.

In this work we focus on single-particle dynamics, embodied in the impurity Green function $G(\omega)$ [the Fourier transform of $G(t) = -\mathrm{i}\langle \hat{T}(c_{\mathrm{i}\sigma}(t) c^{\dagger}_{\mathrm{i}\sigma}) \rangle$]. Analyticity dictates that $G(\omega)$ is specified completely by its spectral function $D(\omega) = -\pi^{-1} \operatorname{sgn}(\omega) G(\omega)$ via

$$G(\omega) = \int_{-\infty}^{\infty} \frac{D(\omega')}{\omega^{+} - \omega'} \mathrm{d}\omega', \tag{2}$$

where $\omega^{+} = \omega + \mathrm{i}0^{+} \operatorname{sgn}(\omega)$.

In the non-interacting ($U = 0$) limit, the Green function is [2]

$$g(\omega) = [\omega^{+} - \epsilon_{\mathrm{i}} - \Delta(\omega)]^{-1} \tag{3}$$

with $\Delta(\omega) = \sum_{\mathbf{k}} |V_{\mathbf{ik}}|^2 [\omega^{+} - \epsilon_{\mathbf{k}}]^{-1}$ the host-impurity hybridization function. Taking $V_{\mathbf{ik}}$ independent of $\mathbf{k}$ for convenience,

$$\Delta(\omega) = V^2 \sum_{\mathbf{k}} P\left(\frac{1}{\omega - \epsilon_{\mathbf{k}}}\right) - \mathrm{i}\pi \operatorname{sgn}(\omega) V^2 \sum_{\mathbf{k}} \delta(\omega - \epsilon_{\mathbf{k}}) \tag{4}$$

$$\equiv \Delta_{\mathrm{R}}(\omega) - \mathrm{i} \operatorname{sgn}(\omega) \Delta_{\mathrm{I}}(\omega). \tag{5}$$

But $\rho(\omega) = \sum_{\mathbf{k}} \delta(\omega - \epsilon_{\mathbf{k}})$ is simply the density of states of the conduction band, so $\Delta_{\mathrm{I}}(\omega) = \pi V^2 \rho(\omega)$. An infinitely-wide, gapped host thus corresponds to a $\Delta_{\mathrm{I}}(\omega)$ of form

$$\Delta_{\mathrm{I}}(\omega) = \begin{cases} \Delta_0 & \text{for } |\omega| > \delta \\ 0 & \text{otherwise} \end{cases} \tag{6}$$

with Δ_0 constant, the corresponding real part following from analyticity as

$$\Delta_{\mathrm{R}}(\omega) = -\frac{\Delta_0}{\pi} \ln \left| \frac{\omega + \delta}{\omega - \delta} \right|. \tag{7}$$

In the general interacting case ($U > 0$) the full Green function is conventionally related to $g(\omega)$ by Dyson's equation

$$G(\omega) = \frac{1}{g(\omega)^{-1} - \Sigma(\omega)}, \tag{8}$$

which defines the (single) self-energy $\Sigma(\omega)$. We note here that the LMA in fact employs a different decomposition of $G(\omega)$, in terms of *two* self-energies, although the single $\Sigma(\omega)$ can of course always be obtained from equation (8) if $G(\omega)$ is known.

Finally, this is a convenient point to define a set of dimensionless parameters that specify the model. We define the dimensionless interaction strength

$$\tilde{U} = \frac{U}{\pi \Delta_0}, \tag{9}$$

and relate the level energy ϵ_{i} to U by means of the asymmetry parameter

$$\eta = 1 + \frac{2\epsilon_{\mathrm{i}}}{U}. \tag{10}$$

For later use we note that the particle-hole–symmetric limit of the model, arising when $\epsilon_{\mathrm{i}} = -U/2$, corresponds to $\eta = 0$ (the host itself is particle-hole symmetric, as above). When specifying the gap δ in Section 5 *ff*, we will usually employ units of the Kondo scale in the absence of the gap.

3 Numerical renormalization group results for the GAIM

Thermodynamics of the GAIM have been calculated by Chen and Jayaprakash (CJ) using a modified NRG approach [11]. The standard method [2] for the metallic AIM relies on a logarithmic discretization of the conduction band, allowing it to be mapped onto an infinite linear chain with exponentially-decreasing coupling constants along the chain. The same procedure can be performed for the GAIM but, because there is a gap in the conduction band, only a finite number of conduction band states are obtained in the logarithmic discretization [11], and the Hamiltonian thus maps onto a finite linear chain. The NRG iterative diagonalisation is thus performed only up to a maximum iteration number $N = N_0$ instead of allowing the calculation to run until the NRG flow tends to a stable fixed point. The final Hamiltonian H_{N_0} obtained from iteration N_0 then describes the low-energy behaviour within the gap, and can be used [11] to obtain the properties of the system on all temperature scales below $T_{N_0} \sim D\Lambda^{-N_0/2}$ (with D the host bandwidth and $\Lambda \gtrsim 1$ the conventional [2] NRG discretization parameter).

The numerical calculations [11] imply that the NRG recovers the basic structure of the quantum phase transition expected [13] from infinite-order perturbation theory in U. In the particle-hole symmetric limit $\epsilon_i = -U/2$, the ground state of the system is found always to be a doublet. Away from particle-hole symmetry by contrast, the ground-state is a Kondo-quenched singlet for sufficiently small gaps but a doublet for larger δ.

More important here are some analytical results arising from the NRG. For the gapped Kondo model with potential scattering, itself obtained from the GAIM under a Schrieffer-Wolff transformation [2] when $U \gg \Delta_0$ and $-\epsilon_i \gg \Delta_0$, CJ have derived effective Hamiltonians valid on energy scales smaller than the gap δ. For $\delta \ll T_K^0$, where T_K^0 is the Kondo temperature in the absence of the gap, the low-energy Hamiltonian takes the form of a pair of orbitals coupled to an impurity spin τ by exchange and potential scattering,

$$H_{\rm eff} = -\tfrac{1}{2}J\tau \cdot f^\dagger_\sigma \sigma_{\sigma\sigma'} f_{\sigma'} + K f^\dagger_\sigma f_\sigma + w(f^\dagger_\sigma g_\sigma + \text{h.c.}) \quad (11)$$

(with a summation convention for repeated spin indices). The renormalized parameters of the effective model turn out to be [11] of the form $J \sim T_K^0$ and $K \sim K_0 T_K^0/D$, with K_0 the 'bare' Schrieffer-Wolff potential scattering, and the 'hopping' $w = \alpha\sqrt{\delta T_K^0}$ (with α a constant of proportionality, determined in practice by fitting to the numerical RG results).

This effective Hamiltonian, equation (11), can be used to derive a number of important results. It is dominated by its three lowest eigenstates, which we label in the form (Q, S) with Q the charge of the system relative to one electron per orbital, and S its total spin. The three lowest states are then the doublet $(0, \frac{1}{2})$ and the singlets $(-1, 0)$ and $(1, 0)$. In the particle-hole symmetric limit [for which $(\pm 1, 0)$ are degenerate], CJ show that the doublet $(0, \frac{1}{2})$ is always the ground state, *i.e.* the system adopts the LM ground state. Away from particle-hole symmetry, for sufficiently small gaps δ/T_K^0, it is by contrast straightforward to show that the ground state is one of the (now non-degenerate) singlets, $(-1, 0)$ or $(1, 0)$, depending on whether $K > 0$ or $K < 0$ respectively. These singlets correspond to the GFL phase of the model. Upon increasing δ/T_K^0 however, there is a level crossing [11] of the ground state with the excited doublet $(0, \frac{1}{2})$, and hence the quantum phase transition to the LM state.

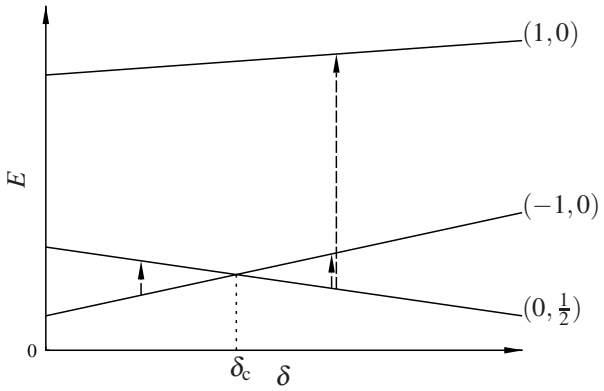

Fig. 1. Schematic representation of the quantum phase transition away from particle-hole symmetry. The three solid lines represent the evolution (with increasing gap, δ) of the energies of the $(0, \frac{1}{2})$ and $(\pm 1, 0)$ states of the effective Hamiltonian equation (11) as discussed in text. The dotted line marks the critical δ_c at which point the lowest two levels cross. The dashed lines show schematically the allowed single-particle excitations from the ground state for both $\delta < \delta_c$ and $\delta > \delta_c$: in the former case, only $(0, \frac{1}{2})$ is accessible; for the latter by contrast, both low-lying excited states can be reached by the addition/removal of a single electron.

At this stage we can make an important deduction from the schematic behaviour of the level crossing, which will ultimately be used to develop the method used within the LMA for the GAIM. Figure 1 shows schematically the energy levels of the effective Hamiltonian equation (11) described above, taking for specificity $K > 0$ such that $(-1, 0)$ is the ground state at small δ/T_K^0. More precisely, $(-1, 0)$ is the ground state for all $\delta < \delta_c$, whereas for $\delta > \delta_c$ the order of the $(-1, 0)$ and $(0, \frac{1}{2})$ levels is interchanged and the latter is hence the ground state. The $(1, 0)$ state remains an excited state for all δ.

Now consider the single-particle excitations of the system from the ground state. For $\delta < \delta_c$, the only possible single-particle excitation within this low-energy manifold is from $(-1, 0)$ to $(0, \frac{1}{2})$. [There is an excitation from $(-1, 0)$ to the $(-2, \frac{1}{2})$ state of Eq. (11), but it is of much higher energy and is irrelevant to the discussion here]. By contrast, as soon as one enters the LM phase for $\delta > \delta_c$, there are two possible low-energy excitations, from $(0, \frac{1}{2})$ to $(\pm 1, 0)$. And although the energy of the transition between $(0, \frac{1}{2})$ and $(-1, 0)$ vanishes as one passes through the phase transition at δ_c, the energy of the $(0, \frac{1}{2}) \rightarrow (1, 0)$ is *finite* as soon as one enters the LM phase. Hence a pole

in the single-particle spectrum of the system occurs *discontinuously* at a finite frequency when one crosses the GFL→LM phase boundary. We shall see that this behaviour can indeed be recovered quite straightforwardly by the two–self-energy description used by the LMA in Section 6.

In addition, a useful result [11] can be obtained from equation (11) in the particle-hole–symmetric limit. As mentioned above, in this case the $(0, \frac{1}{2})$ LM state is the ground state for all δ, and the two excited states $(\pm 1, 0)$ are degenerate. One can calculate perturbatively the excitation energy from $(0, \frac{1}{2})$ to $(\pm 1, 0)$ as shown in [11]: the result is that

$$\Delta E \sim \frac{w^4}{J^3} \propto \frac{\delta^2}{T_{\rm K}^0} \tag{12}$$

for small w. Since the energy gap corresponds to the frequency at which poles arise (symmetrically) in the single particle spectrum $D(\omega)$, this result provides a benchmark for any approximation to the single-particle dynamics.

Finally, we can draw a general conclusion from the NRG analysis of the GAIM. We explained above how the NRG is in essence identical to that of the metallic AIM for iteration numbers $N \leq N_0$ (corresponding to energy scales $\gtrsim \delta$). This means that both the thermodynamics of the GAIM for $T \gg \delta$, *and* its dynamics for $\omega \gg \delta$, will be essentially unchanged from those of the parent metallic AIM. This is an important argument. In particular, if $\delta \ll T_{\rm K}^0$ then it follows that the gapped system will appear to display the same Kondo physics as the metallic case, with deviations arising only on the lowest energy scales of the order of the gap (for example, one would still expect to see the vast majority of the characteristic Kondo resonance in the single-particle spectrum). We will make use of this argument throughout the paper; in particular it will be used to obtain the self-consistency criterion for the LMA in the LM phase (see Sect. 4.2).

4 Local moment approach to the GAIM

The LMA [14–16] centres on a two–self-energy description of the local impurity propagator. Such a description arises naturally at the mean-field level of unrestricted Hartree Fock (UHF) [1], where the two self-energies are the 'static' Fock bubble diagrams that represent the interaction between the added/removed σ-spin electron and each of the two broken-symmetry mean-field ground states. The LMA overcomes the intrinsic deficiencies of crude static mean-field theory by introducting additional, dynamical contributions to the self-energies. These describe low-energy tunnelling processes between the locally degenerate mean-field states, and as such allow for the possibility of restoration of broken symmetry and hence recovery of Fermi liquid behaviour at low-energies.

We point out here that the broken-symmetry arising at mean-field level is naturally restored on the lowest frequency scales, while at higher frequencies the symmetry remains effectively broken and the two LMA Green functions $G_\uparrow(\omega)$ and $G_\downarrow(\omega)$ are distinct. Such a broken-symmetry description of the Kondo physics arising in a GFL phase is known from other theories, notably in NRG where at high frequencies the physics is controlled by the broken-symmetry 'local moment' fixed point (the present authors have in fact shown [24] that the same two–self-energy description used within the LMA arises also in the NRG). Likewise, Anderson, Yuval and Hamann's [25] pioneering description of the Kondo effect—in which the problem is viewed as a one-dimensional gas of spin-flips propagating in time—is also fundamentally a broken-symmetry approach: on short timescales (high frequencies) the impurity spin is either $\uparrow$ or $\downarrow$, and only on longer timescales on the order of $\hbar/T_{\rm K}^0$ is symmetry restored and the Kondo singlet formed.

Moreover, we add [18] that in order to describe a quantum phase transition between a GFL phase and a broken-symmetry LM phase, the underlying theory must be sufficiently general to capture *both* phases: one cannot hope to obtain a satisfactory description of a broken-symmetry phase using a theory which *a priori* requires the ground state to be a singlet. To this end the two self-energy description inherent to the LMA, combined with the possibility of symmetry restoration at low-energies, is a necessity.

To implement the LMA for the GAIM, we follow the preliminary analysis of reference [15]. The Green function $G(\omega)$ is written as the (rotationally invariant) average of two broken-symmetry propagators

$$G(\omega) = \tfrac{1}{2}\left[G_\uparrow(\omega) + G_\downarrow(\omega)\right], \tag{13}$$

each of which is expressed in terms of a Dyson equation

$$G_\sigma(\omega) = \frac{1}{g(\omega)^{-1} - \tilde{\Sigma}_\sigma(\omega)} \tag{14}$$

with $\tilde{\Sigma}_\uparrow(\omega)$ and $\tilde{\Sigma}_\downarrow(\omega)$ the two self-energies. These are constructed from mean-field-like propagators

$$\mathcal{G}_\sigma(\omega) = \left[\omega^+ - e_{\rm i} - \tfrac{1}{2}\sigma U|\mu| - \Delta(\omega)\right]^{-1} \tag{15}$$

in which the mean-field parameters $e_{\rm i}$ and $|\mu|$ are determined by a pair of appropriate self-consistency conditions (to be described in detail later). The self-energies are separated into a static contribution $\tilde{\Sigma}_\sigma^0$ (*i.e.* the sole contribution at UHF level) plus a dynamical piece $\Sigma_\sigma(\omega) = \Sigma_\sigma^{\rm R}(\omega) - {\rm i}\,{\rm sgn}(\omega)\Sigma_\sigma^{\rm I}(\omega)$,

$$\tilde{\Sigma}_\sigma(\omega) = \tilde{\Sigma}_\sigma^0 + \Sigma_\sigma(\omega). \tag{16}$$

The static self-energies are given diagrammatically by the Fock bubble [14], which translates simply as

$$\tilde{\Sigma}_\sigma^0 = U\int_{-\infty}^{0} {\rm d}\omega\; D_{-\sigma}^0(\omega). \tag{17}$$

with

$$D_\sigma^0(\omega) = -\frac{1}{\pi}\,{\rm sgn}(\omega)\,{\rm Im}\,\mathcal{G}_\sigma(\omega). \tag{18}$$

The dynamical self-energies are approximated by the RPA particle-hole ladder sum [14]. Specifically, for $\Sigma_\downarrow(\omega)$,

$$\Sigma_\downarrow(\omega) = \frac{U^2}{2\pi \mathrm{i}} \int_{-\infty}^{\infty} \mathrm{d}\omega_1 \; \Pi^{+-}(\omega_1)\mathcal{G}_\uparrow(\omega - \omega_1), \tag{19}$$

where $\Pi^{+-}(\omega)$ is the transverse spin-polarisation propagator

$$\Pi^{+-}(\omega) = \frac{{}^0\Pi^{+-}(\omega)}{1 - U\,{}^0\Pi^{+-}(\omega)}, \tag{20}$$

and

$${}^0\Pi^{+-}(\omega) = \frac{\mathrm{i}}{2\pi} \int_{-\infty}^{\infty} \mathrm{d}\omega_1 \; \mathcal{G}_\downarrow(\omega_1)\mathcal{G}_\uparrow(\omega_1 - \omega). \tag{21}$$

Likewise, $\Sigma_\uparrow(\omega)$ is obtained from the analogues of equations (19)–(21) with $\uparrow$ and $\downarrow$ interchanged.

As noted previously [14,15], analyticity of $\Pi^{+-}(\omega)$ places restrictions on the choice of $|\mu|$ and e_i. The $(e_\mathrm{i}, |\mu|)$ plane is found to divide into 'stable' and 'unstable' regions, the border between which corresponds to the line of solutions one would obtain from pure UHF alone, $|\mu| = |\mu_0(e_\mathrm{i})|$ (see Fig. 2 of Ref. [15]). It is implicit in the following that the e_i and $|\mu|$ used are always chosen to satisfy this analyticity requirement.

The stability border has however a further significance within the LMA. If one chooses $|\mu| = |\mu_0(e_\mathrm{i})|$, *i.e.* a point *on* the stability border, it is readily shown [14,15] that $\mathrm{Im}\Pi^{+-}(\omega)$ has a pole at $\omega = 0$ identically. Upon moving away from the border into the stable region, the pole is found to shift to a positive, finite frequency (ultimately becoming a sharp resonance deeper in the stable region). As for the gapless (metallic) AIM [14,15], we use the position of this low-energy excitation (pole or resonance) in $\mathrm{Im}\Pi^{+-}(\omega)$ to define the Kondo scale for the GAIM, and henceforth denote this scale ω_m.

From the overview given above, the reader will notice that the basic structure of the LMA Green functions used in this work—including the particular class of dynamical self-energy diagrams summed in practice—remains unchanged from that used in reference [15]. The most significant difference in the LMA for the GAIM is the choice of $|\mu|$ and e_i, as we now explain. It turns out that one requires different self-consistency criteria for the two phases, GFL and LM. The former is in fact the simpler of the two, and we thus consider it first.

4.1 LMA for the GFL phase

In the GFL phase, the usual LMA procedures of symmetry restoration and satisfaction of the Friedel sum rule [15] can be used to determine $|\mu|$ and e_i completely and uniquely. We follow the approach described in section 4 of reference [15], employing the symmetry restoration condition,

$$\tilde{\Sigma}_\uparrow(\omega = 0) = \tilde{\Sigma}_\downarrow(\omega = 0), \tag{22}$$

and using the generalized Friedel sum rule appropriate to the GAIM [13] (which itself follows from the Luttinger integral theorem [13])

$$n_\mathrm{imp} = 1 - \mathrm{sgn}(\epsilon_\mathrm{i}^*) \tag{23}$$

where $\epsilon_\mathrm{i}^* = \epsilon_\mathrm{i} + \Sigma_\mathrm{R}(0)$ is the renormalized level energy of the impurity. n_imp is the change in number of electrons in the system due to addition of the impurity [2] (given explicitly by Eq. (24) below). Note that, in contrast to the gapless AIM [2] where n_imp can vary continuously between 0 and 2, equation (23) shows that n_imp for the GAIM can take only the discrete values 0 or 2, according to whether the renormalized level $\epsilon_\mathrm{i}^* > 0$ or < 0 respectively.

In practice, the frequency integral [2]

$$n_\mathrm{imp} = \mathrm{Im}\,\frac{2}{\pi} \int_{-\infty}^{0} \mathrm{d}\omega \; \left[1 - \frac{\partial \Delta(\omega)}{\partial \omega}\right] G(\omega) \tag{24}$$

for n_imp is rather sensitive to numerical errors. In order to make the calculation stable, we first separate the integrand into its real and imaginary parts. Using equation (5) for $\Delta(\omega)$,

$$\frac{\partial \Delta(\omega)}{\partial \omega} = \frac{\partial \Delta_\mathrm{R}(\omega)}{\partial \omega} - \mathrm{i}\Delta_0 \,\mathrm{sgn}(\omega)\left[\delta(\omega + \delta) + \delta(\omega - \delta)\right], \tag{25}$$

where the explicit form of $\Delta_\mathrm{I}(\omega)$ (Eq. (6)) has been used. Substituting equation (25) into equation (24), it can then be shown that

$$n_\mathrm{imp} = \frac{\Delta_0}{\pi} \sum_\sigma \mathrm{Re}\, G_\sigma(-\delta) + \sum_\sigma \int_{-\infty}^{0} \mathrm{d}\omega \; D_\sigma(\omega) \left[1 - \frac{\partial \Delta_\mathrm{R}(\omega)}{\partial \omega}\right], \tag{26}$$

with the LMA $G_\sigma(\omega)$ defined by equation (14) and $D_\sigma(\omega) = -\pi^{-1}\,\mathrm{sgn}(\omega)\mathrm{Im}G_\sigma(\omega)$. The ω-integral of $\sum_\sigma D_\sigma(\omega)$ gives the number of electrons on the impurity, n_i, and from the explicit form of $\Delta_\mathrm{R}(\omega)$ in equation (7) it follows that

$$n_\mathrm{imp} = n_\mathrm{i} + \frac{\Delta_0}{\pi} \sum_\sigma \mathrm{Re}\, G_\sigma(-\delta) + \frac{\Delta_0}{\pi} \sum_\sigma \left[\int_{-\infty}^{0} \mathrm{d}\omega \; \frac{D_\sigma(\omega)}{\omega + \delta} + \int_{-\infty}^{0} \mathrm{d}\omega \; \frac{D_\sigma(\omega)}{\omega - \delta}\right]. \tag{27}$$

Then, by noting that the integrals in the second line are related to the one-sided Hilbert transforms of the LMA spectra,

$$G_\sigma^\pm(\omega) = \int_{-\infty}^{\infty} \mathrm{d}\omega_1 \; \frac{D_\sigma(\omega_1)\theta(\pm\omega_1)}{\omega - \omega_1 \pm \mathrm{i}0^+} \tag{28}$$

(with $\theta(x)$ the unit step function), and using equation (2) to write $G_\sigma(-\delta) = G_\sigma^+(-\delta) + G_\sigma^-(-\delta)$, one can simplify equation (27) to

$$n_\mathrm{imp} = n_\mathrm{i} + \frac{\Delta_0}{\pi} \sum_\sigma \left[\mathrm{Re}\, G_\sigma^+(-\delta) + \mathrm{Re}\, G_\sigma^-(\delta)\right]. \tag{29}$$

This is the equation from which $n_{\rm imp}$ is calculated in practice, with the real parts of $G^{\pm}_{\sigma}(\omega)$ obtained from equation (28), and $n_{\rm i}$ obtained from direct integration of the impurity spectrum.

The mean-field parameters $|\mu|$ and $e_{\rm i}$ are readily determined for the GFL phase. For given 'bare' model parameters U, $\epsilon_{\rm i}$ and δ, and a chosen $e_{\rm i}$, the local moment $|\mu|$ is obtained by varying it until the symmetry restoration condition equation (22) is satisfied. $n_{\rm imp}$ is then calculated from equation (29), and $e_{\rm i}$ itself is varied (ensuring symmetry restoration at each step) until the resultant $n_{\rm imp} = 0$ or 2 as required from the generalized Friedel sum rule equation (23).

Before moving to the LM phase, we add that we shall assume the system adopts the GFL phase whenever symmetry-restored solutions with $n_{\rm imp} = 0$ or 2 can be found. This naturally provides the criterion for determining the phase boundary between GFL and LM phases: if one gradually increases δ from zero at fixed U and η $(= 1 + 2\epsilon_{\rm i}/U)$, then the point at which GFL solutions of the above form cease to exist marks the quantum phase transition to the LM phase. In Section 6.1, we shall see that this approach leads to an excellent description of the phase boundary between the GFL and LM phases.

4.2 LMA for the LM phase

Determining $|\mu|$ and $e_{\rm i}$ within the LM phase requires a significant extension of the LMA. The perturbative results that lead to symmetry restoration and the generalized Friedel sum rule obviously do not apply within the LM phase [13], and hence new criteria are required to determine $|\mu|$ and $e_{\rm i}$ in this phase. We begin with the particle-hole–symmetric limit ($\epsilon_{\rm i} = -U/2$), since in this case $e_{\rm i}$ vanishes by symmetry and hence only a condition on $|\mu|$ is required. Once the basic method has been explained, we shall see that it is naturally extendible to the LM phase away from particle-hole symmetry.

4.2.1 Particle-hole–symmetric LM phase

Previous LMA studies of non-Fermi-liquid behaviour have centered on the pseudogap Anderson model [17–20] (PAIM, for which $\Delta_{\rm I} \propto |\omega|^r$ has a soft gap at the Fermi level). In the particle-hole–symmetric PAIM, for $0 < r < \frac{1}{2}$, the system evolves adiabatically from the non-interacting limit into a GFL phase as U is increased from zero. This GFL phase persists with increasing U up to a finite critical $U_{\rm c}$, at which the system undergoes a quantum phase transition to the LM phase (which behaviour is qualitatively different from that of the GAIM at particle-hole symmetry, where the critical $U_{\rm c} = 0$). One describes the GFL phase of the PAIM in much the same way as discussed in the previous section for the GAIM; $e_{\rm i} = 0$ by symmetry, with the value of $|\mu|$ determined by the imposition of symmetry restoration. As U is increased inside the GFL phase, the resultant $|\mu|$ tends toward the UHF value $|\mu_0|$ at $U_{\rm c}$. Above $U_{\rm c}$ symmetry restoration is not possible

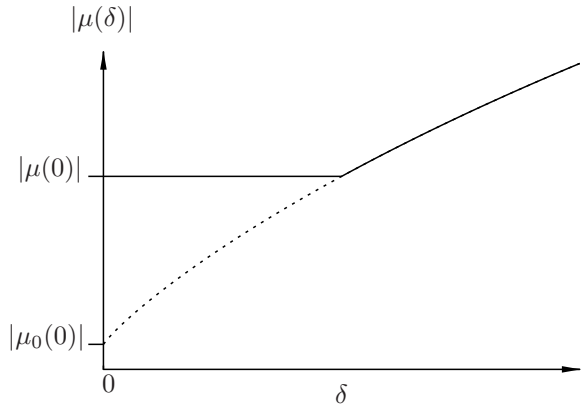

Fig. 2. Schematic illustration of the procedure for choosing the moment $|\mu|$ in the LM phase that arises ubiquitously for the particle-hole–symmetric limit of the GAIM. The solid line represents the chosen $|\mu(\delta)|$; the dotted line represents the UHF moment $|\mu_0(\delta)|$.

for any stable $|\mu|$ (whence $U = U_{\rm c}$ is the quantum critical point where the system undergoes the transition to the LM phase). To describe the LM phase that persists for all $U > U_{\rm c}$, one simply sets $|\mu| = |\mu_0|$ throughout, which means that $|\mu|$ is continuous across the phase boundary. The physical basis for this is that when $|\mu| = |\mu_0|$, the pole in $\mathrm{Im}\,\Pi^{+-}(\omega)$ lies at $\omega = 0$ (see Sect. 4 above). This represents a zero energy cost for flipping the impurity spin, as expected for a doubly-degenerate LM phase.

From the discussion above, one might therefore expect that the LM phase of the GAIM should likewise be described within the LMA by setting $|\mu|$ to the UHF value $|\mu_0|$ throughout. This is not however the case, as can be explained using a simple argument.

Consider how the system behaves when an infinitesimal gap δ is opened in the conduction band, for some fixed $U > 0$. The NRG analysis [11] discussed previously makes it clear what the outcome should be. An infinitesimal gap will make essentially no difference to the coupling constants of the discretized linear-chain Hamiltonian, and hence the NRG will lead to the same results known [2,14,15] to arise when $\delta = 0$, except on the frequency scales $\omega \lesssim \delta$ (here infinitesimal by construction). In particular, all manifestations of the Kondo effect—including the Kondo resonance in the single particle spectrum of width $\sim T_{\rm K}$—will be affected only on these very lowest of frequency scales, and will appear otherwise unchanged.

It is now not difficult to see why setting $|\mu| = |\mu_0|$ throughout the LM phase of the GAIM is incorrect (with reference to Fig. 2, which provides a schematic illustration of the basic ideas involved). In the metallic AIM, where $\delta = 0$, the LMA moment $|\mu(\delta = 0)|$ is determined by symmetry restoration. This moment lies above the corresponding UHF value $|\mu_0(\delta = 0)|$ (the dotted line in Fig. 2) by an amount proportional [14] to $T_{\rm K}^0/U$, and hence from the discussion of Section 4 generates the exponentially-small Kondo scale $T_{\rm K}^0$ within the LMA. Now, if one were

simply to set $|\mu(\delta)| = |\mu_0(\delta)|$ for any finite δ, no matter how small, there would be a discontinuous drop in $|\mu(\delta)|$ upon opening the gap. [1] Such a drop in $|\mu(\delta)|$ would lead to qualitative differences between the LMA spectra at $\delta = 0$ and $\delta = 0^+$—on *all* frequency scales, not just those of the order of the gap and below—and as such must therefore be incorrect.

What is clear instead is that the LMA $|\mu(\delta)|$ must evolve *continuously* from its value at $\delta = 0$, as this will recover the correct behaviour at $\omega \gg \delta$ for infinitesimally-small gaps. To this end we simply set $|\mu(\delta)| = |\mu(\delta = 0)|$, with a caveat explained below. In Section 5.1 we show that, in addition to leaving the single-particle spectrum essentially unchanged on frequency scales $\omega \gg \delta$, this choice of $|\mu(\delta)|$ more importantly recovers the correct $\delta \to 0$ behaviour *inside* the gap, $\omega < \delta$, as known from the NRG studies [11] of Chen and Jayaprakash.

The caveat pertains to the case when δ is 'large'—which in practice means δ much greater than the Kondo scale in the absence of the gap, $\omega_{\rm m}^0 \equiv \omega_{\rm m}(\delta = 0)$. This is because $|\mu(\delta)|$ must be larger than $|\mu_0(\delta)|$ for stability, but the latter increases monotonically with δ and therefore crosses $|\mu(\delta = 0)|$ at some finite δ (see Fig. 2). To avoid the instability that arises if $|\mu(\delta)| < |\mu_0(\delta)|$ (see Sect. 4), we simply set $|\mu(\delta)| = |\mu_0(\delta)|$ at and above this gap. $|\mu(\delta)|$ is thus given throughout the particle-hole–symmetric LM phase by

$$|\mu(\delta)| = \max\left(|\mu(0)|, |\mu_0(\delta)|\right), \tag{30}$$

as shown schematically by the solid line in Figure 2.

Before explaining how this procedure is generalized to the particle-hole–asymmetric case, we add further that equation (30) is physically natural for $|\mu(\delta)|$ when the gap is large compared to $\omega_{\rm m}^0$ and $\tilde{U} \gg 1$. This is because, upon increasing δ from zero, the UHF $|\mu_0(\delta)|$ rises sufficiently rapidly with δ that equation (30) gives $|\mu(\delta)| = |\mu_0(\delta)|$ whenever $\delta \gg \omega_{\rm m}^0$. The pole in $\mathrm{Im}\, \Pi^{+-}(\omega)$ then lies at $\omega = 0$, reflecting the fact that when $\delta \gg \omega_{\rm m}^0$, the dominant transverse spin-excitation is the zero-frequency 'Goldstone mode' associated with flipping the doubly-degenerate impurity LM state; any remnants of the Kondo effect and its associated Kondo scale $\omega_{\rm m}^0$ are destroyed by the gap. Although the precise behaviour in the intermediate regime, $\delta \sim \omega_{\rm m}^0$ is less obvious, we simply argue that equation (30) is a sensible choice for $|\mu(\delta)|$ that bridges the known $\delta \ll \omega_{\rm m}^0$ and $\delta \gg \omega_{\rm m}^0$ behaviour in a physically realistic manner.

4.2.2 Particle-hole–asymmetric LM phase

The LM phase away from particle-hole asymmetry can be handled using a straightforward generalisation of the above procedure; enabling calulation of the LMA spectra for any choice of the bare parameters $\tilde{U}$, η and $\tilde{\delta}$ (considered explicitly in Sect. 6). The motivation for our approach is the discontinuity across the phase boundary, discussed in Section 3 and illustrated schematically in Figure 1; which can be captured by the LMA due to its inherent two–self-energy description.

Let us consider the evolution of the system with increasing δ away from particle-hole symmetry. For sufficiently small gaps as seen in Figure 1, the system adopts the GFL phase and there is correspondingly only one low-energy single-particle excitation on energy scales below δ. This is reflected by the single pole in $D(\omega)$ known from perturbation theory [13]. As one approaches the phase boundary from the GFL side, it follows from Figure 1 that the position of this pole must tend to $\omega = 0$. Hence, from equation (13), equation (14) and equation (3), *both* self-energies must satisfy

$$\epsilon_{\rm i} + \tilde{\Sigma}_\sigma(0) \to 0 \quad \text{as } \delta \to \delta_{\rm c}^-. \tag{31}$$

On the other side of the transition, $\delta = \delta_{\rm c}^+$ however, the behaviour is very different. As seen in Figure 1, there are now *two* poles. The one corresponding to the (now reversed) excitation seen in the GFL phase remains at a vanishingly-small energy difference, but an additional pole also arises at a finite frequency. This requires that either

$$\epsilon_{\rm i} + \tilde{\Sigma}_\uparrow(0) \to 0 \quad \text{and} \quad \epsilon_{\rm i} + \tilde{\Sigma}_\downarrow(0) \neq 0 \quad \text{as } \delta \to \delta_{\rm c}^+, \tag{32}$$

or

$$\epsilon_{\rm i} + \tilde{\Sigma}_\downarrow(0) \to 0 \quad \text{and} \quad \epsilon_{\rm i} + \tilde{\Sigma}_\uparrow(0) \neq 0 \quad \text{as } \delta \to \delta_{\rm c}^+. \tag{33}$$

We thus conclude that one of the self-energies $\tilde{\Sigma}_\sigma(0)$ must be *discontinuous* across the GFL $\leftrightarrow$ LM phase boundary. This result is central to the LMA for the LM phase away from particle-hole symmetry.

LM phase at $\delta_{\rm c}^+$

For given U and $\epsilon_{\rm i}$ (or η), the critical gap $\delta_{\rm c}$ above which GFL-phase solutions no longer exist is obtained as described in Section 4.1; such that in the GFL phase at $\delta = \delta_{\rm c}^-$, equation (31) holds for both $\sigma = \uparrow$ and $\downarrow$.

Now consider moving across the phase boundary to $\delta_{\rm c}^+$. It is necessary now to determine self-consistently the new values of both $|\mu|$ and $e_{\rm i}$ at this point, which we do as follows: $|\mu|$ is determined by varying it until

$$\epsilon_{\rm i} + \tilde{\Sigma}_\sigma(0) \to 0 \tag{34}$$

is satisfied for either $\sigma = \uparrow$ or $\sigma = \downarrow$ (*i.e.* until one or other of Eq. (32) or Eq. (33) is satisfied[2]); and $e_{\rm i}$ is determined by requiring simultaneously that $n_{\rm imp} = 1$ (with $n_{\rm imp}$ calculated from Eq. (29)).

[1] The value of $|\mu_0(\delta)|$ evolves smoothly and continuously with increasing δ from its value at $\delta = 0$.

[2] We note that there is no ambiguity associated with the choice of σ in equation (34): in practice, self-consistent solutions with $n_{\rm imp} = 1$ are found to arise only for one of $\sigma = \uparrow$ or $\sigma = \downarrow$.

The condition $n_{\rm imp} = 1$ is certainly non-trivial away from particle-hole symmetry. It has been shown [18] to arise for the LM phase of the PAIM; and we impose it here for similar reasons, reflecting as it does perturbative continuity (in the host-impurity coupling V) of the LM phase from the *atomic* limit (where $n_{\rm imp} = 1$ arises for any $\epsilon_{\rm i} < 0$ and $\epsilon_{\rm i} + U > 0$). In addition, not only is an integral $n_{\rm imp}$ physically natural for a system with a gapped density-of-states but, as for the PAIM [18], it turns out that $n_{\rm imp} = 1$ is in fact the only possible integral value for which self-consistent solutions of the above form can be found.

LM phase for $\delta > \delta_{\rm c}$

Once the self-consistent $|\mu|$ and $e_{\rm i}$ are known for $\delta = \delta_{\rm c}^{+}$, we then extend the LMA method used in the particle-hole–symmetric limit (Section 4.2.1 above). We remarked above that the physics of the problem known from NRG is recovered in the particle-hole–symmetric limit if one chooses $|\mu(\delta)|$ according to equation (30). We now extend this to the general particle-hole asymmetric case by requiring that one fixes both $|\mu(\delta)|$ and $e_{\rm i}$ at their values obtained self-consistently at $\delta_{\rm c}^{+}$ [again with the same proviso that $|\mu(\delta)|$ is instead set to $|\mu_0(\delta)|$ when the latter becomes larger than $|\mu(\delta_{\rm c}^{+})|$]. Such an approach is the natural generalisation of the procedure used in the particle-hole symmetric limit, in which case $\delta_{\rm c} = 0$ and $e_{\rm i} = 0$ are known from the outset. In Section 6 we present numerical results using this approach, and show that they too are consistent with the behaviour known from NRG [11].

5 Analytic results at particle-hole symmetry

Before considering the numerics, we discuss some important asymptotic results that can be obtained analytically at particle-hole symmetry ($\epsilon_{\rm i} = -U/2$) where the LM phase arises for all $\delta > 0$. Our focus here is naturally the strong coupling ('Kondo') regime $\tilde{U} = U/\pi\Delta_0 \gg 1$, with the gap δ taken to be any finite multiple of the low-energy Kondo scale in the absence of the gap, $\omega_{\rm m}^0 = \omega_{\rm m}(\delta = 0)$; and with $\omega_{\rm m}^0$ known from the LMA for the metallic AIM [14] as

$$\omega_{\rm m}^0 = \beta U \exp\left(\frac{-\pi^2}{8}\tilde{U}\right) \tag{35}$$

(with β a pure constant $\mathcal{O}(1)$), which we add gives the exact exponential dependence of the Kondo scale [2,14]. In what follows, $\tilde{\delta} = \delta/\omega_{\rm m}^0$.

With $\tilde{\omega} = \omega/\omega_{\rm m}^0$, the two key results here are for the frequency-dependence of the LMA self-energies:

$$-\frac{U}{2} + \tilde{\Sigma}_{\uparrow}^{\rm R}(\omega) \overset{\tilde{U}\gg 1}{\sim} -\frac{4\Delta_0}{\pi}\ln\left(\tilde{\omega} + \tilde{\delta} + 1\right) \tag{36}$$

and

$$\tilde{\Sigma}_{\uparrow}^{\rm I}(\omega) \overset{\tilde{U}\gg 1}{\sim} 4\theta\left[-(\tilde{\omega} + \tilde{\delta} + 1)\right]\Delta_0. \tag{37}$$

These equations hold for finite $\tilde{\omega} = \omega/\omega_{\rm m}^0$ in the formal strong coupling limit where $\omega_{\rm m}^0 \to 0$. Their derivation is given in the Appendix; here we take them as given.

5.1 Strong-coupling behaviour of the single-particle spectrum

It is now of course straightforward to obtain the spectrum $D(\omega)$ in closed form. We simply employ the asymptotic forms of the self-energy equation (36) and equation (37) in the Dyson equation (14). Since we have specified only $\tilde{\Sigma}_{\uparrow}(\omega)$ above, it will be convenient to use the symmetry $D_{\uparrow}^0(\omega) = D_{\downarrow}^0(-\omega)$ to write $D(\omega) = D(-\omega)$ in terms of $D_{\uparrow}(\omega)$ only, *i.e.*

$$D(\omega) = \tfrac{1}{2}\left[D_{\uparrow}(|\omega|) + D_{\uparrow}(-|\omega|)\right]. \tag{38}$$

It is then readily shown that the band contribution to $D(\omega)$ is

$$\pi\Delta_0{}^b D(\tilde{\omega}) = \frac{\frac{1}{2}\theta(|\tilde{\omega}| - \tilde{\delta})}{\left[A(\tilde{\omega},\tilde{\delta})\right]^2 + 1} + \frac{\frac{1}{2}\left[\theta(|\tilde{\omega}| - \tilde{\delta}) + 4\theta(|\tilde{\omega}| - \tilde{\delta} - 1)\right]}{\left[B(\tilde{\omega},\tilde{\delta})\right]^2 + \left[1 + 4\theta(|\tilde{\omega}| - \tilde{\delta} - 1)\right]^2}, \tag{39}$$

with

$$A(\tilde{\omega},\tilde{\delta}) = \frac{1}{\pi}\ln\left(\frac{|\tilde{\omega}| + \tilde{\delta}}{|\tilde{\omega}| - \tilde{\delta}}\right) + \frac{4}{\pi}\ln(|\tilde{\omega}| + \tilde{\delta} + 1) \tag{40}$$

and

$$B(\tilde{\omega},\tilde{\delta}) = \frac{1}{\pi}\ln\left(\frac{|\tilde{\omega}| - \tilde{\delta}}{|\tilde{\omega}| + \tilde{\delta}}\right) + \frac{4}{\pi}\ln(|\tilde{\omega}| - \tilde{\delta} - 1). \tag{41}$$

Inside the gap there are of course two symmetrically distributed poles at $\tilde{\omega} = \pm\tilde{\omega}_{\rm p}$, with $|\tilde{\omega}_{\rm p}| < \tilde{\delta}$. These are given by solution of $\omega + \frac{U}{2} - \Delta_{\rm R}(\omega) - \tilde{\Sigma}_{\sigma}^{\rm R}(\omega) = 0$ (where the 'bare' $\omega = \tilde{\omega}\omega_{\rm m}^0 \equiv 0$); and hence from equation (36) and equation (7) by

$$\ln\left(\frac{\tilde{\omega}_{\rm p} + \tilde{\delta}}{\tilde{\delta} - \tilde{\omega}_{\rm p}}\right) + 4\ln(\tilde{\omega}_{\rm p} + \tilde{\delta} + 1) = 0, \tag{42}$$

or equivalently

$$(\tilde{\omega}_{\rm p} + \tilde{\delta})(\tilde{\omega}_{\rm p} + \tilde{\delta} + 1)^4 = \tilde{\delta} - \tilde{\omega}_{\rm p}. \tag{43}$$

On increasing $\tilde{\omega}$ inside the gap from $-\tilde{\delta}$ to $+\tilde{\delta}$, the left-hand side of equation (43) increases monotonically from 0 to $2\tilde{\delta}(2\tilde{\delta}+1)^4$, while the right-hand side decreases from $2\tilde{\delta}$ to 0. Hence there is always one solution of equation (43) inside the gap (*i.e.* for $|\tilde{\omega}_{\rm p}| < \tilde{\delta}$); and it is simple to show that it corresponds to $\tilde{\omega}_{\rm p} < 0$.

We see directly from equations (39) and (42) that for any particular choice of $\tilde{\delta} = \delta/\omega_{\rm m}^0$, the single-particle spectrum is solely a function of $\tilde{\omega} = \omega/\omega_{\rm m}^0$. Hence there is a *scaling spectrum* for each $\tilde{\delta}$, onto which the numerical finite-$\tilde{U}$ LMA spectrum will collapse when plotted against $\omega/\omega_{\rm m}^0$ for sufficiently strong coupling $\tilde{U}$. In Section 6 we show numerical calculations for the LMA at

finite $\tilde{U}$, which confirm the existence and form of the scaling spectrum.

Before that however, there are two important conclusions that may be drawn from the asymptotic forms of equation (39) and equation (43). The first such result is for the low-frequency pole behaviour inside the gap, which enables comparison of the LMA description of the GAIM to that from NRG [11].

5.1.1 Strong coupling behaviour inside the gap for $\tilde{\delta} \ll 1$

Using equation (43), we now show that in strong-coupling, the LMA expression for the pole position in $D(\omega)$ reduces to the same result obtained by Chen and Jayaprakash in their NRG study of the problem [11].

When $\tilde{\delta} \ll 1$, the pole position $|\tilde{\omega}_{\rm p}| \ll 1$, and hence equation (43) can be expanded to leading order to give $(\tilde{\omega}_{\rm p} + \tilde{\delta})[1 + 4(\tilde{\delta} + \tilde{\omega}_{\rm p})] = \tilde{\delta} - \tilde{\omega}_{\rm p}$; which simplifies to

$$2\tilde{\delta}^2 = -\tilde{\omega}_{\rm p}(1 + 4\tilde{\delta} + 2\tilde{\omega}_{\rm p}) \tag{44}$$

and hence for $\tilde{\delta} \ll 1$ gives

$$|\tilde{\omega}_{\rm p}| = 2\tilde{\delta}^2. \tag{45}$$

Since $\omega_{\rm m}^0$ is proportional to the Kondo temperature in the absence of the gap, $T_{\rm K}^0$, equation (45) gives $|\omega_{\rm p}| \propto \delta^2/T_{\rm K}^0$. *This result is precisely the form obtained by NRG, as discussed in Section 3* (see Eq. (12)). The LMA therefore recovers the correct low-ω behaviour inside the gap of the particle-hole symmetric LM phase. Such a result is certainly non-trivial, and provides further support for the validity of our LMA scheme in the LM phase.

5.1.2 Behaviour of the scaling spectrum for $\tilde{\omega} \gg 1$

The second result that follows directly from equation (39) is the large-$\tilde{\omega}$ behaviour of the scaling spectrum. When $|\tilde{\omega}| \gg \tilde{\delta}$ it is straightforward to see that

$$\pi\Delta_0 D(\tilde{\omega}) \overset{|\tilde{\omega}|\gg\tilde{\delta}}{=} \frac{\frac{1}{2}}{\frac{16}{\pi^2}\ln^2(|\tilde{\omega}|+1)+1} + \frac{\frac{1}{2}\left[1+4\theta(|\tilde{\omega}|-1)\right]}{\frac{16}{\pi^2}\ln^2(|\tilde{\omega}|-1)+\left[1+4\theta(|\tilde{\omega}|-1)\right]^2}. \tag{46}$$

This is precisely the form of the LMA scaling spectrum for the *metallic* AIM [16] (which itself gives excellent agreement with NRG calculations [16,24]). In other words, on frequency scales much larger than the gap, the physics of the system is effectively the same as it would be if the gap were not present. Such behaviour is correct, following directly from the overview of the NRG procedure in Section 3: the NRG for the GAIM is identical to that for the metallic AIM on energy scales much greater than that of the gap, and hence all physical properties obtained for these energy scales will be independent of whether or not the gap actually exists.

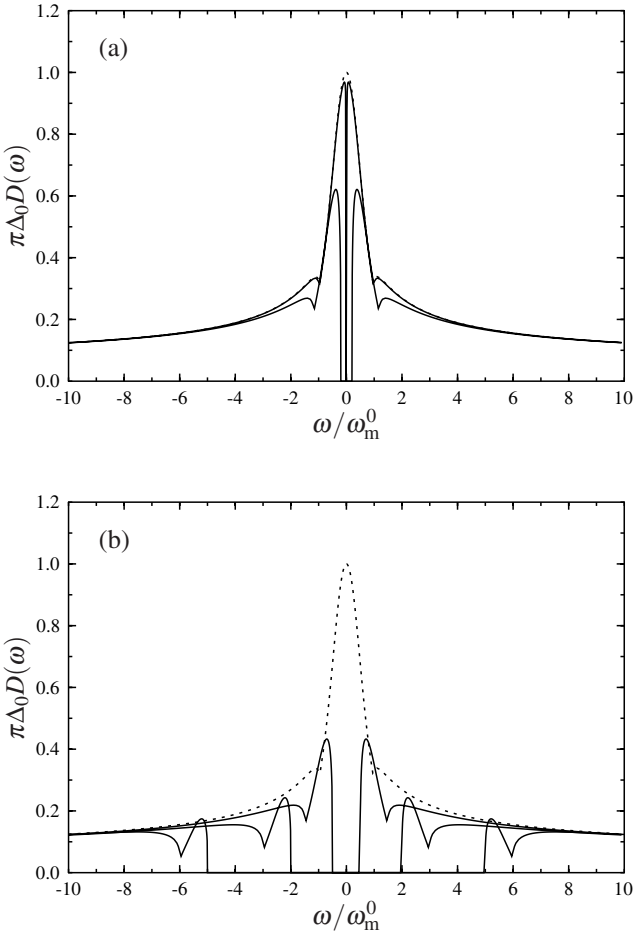

Fig. 3. LMA scaling spectrum for the particle-hole symmetric GAIM, $\pi\Delta_0 D(\omega)$ versus $\tilde{\omega} = \omega/\omega_{\rm m}^0$. The dotted line shows the gapless spectrum, $\delta = 0$. The solid lines are for gaps $\tilde{\delta} = \delta/\omega_{\rm m}^0 = 0.01$ and 0.2 ((a)), and 0.5, 2 and 5 ((b)), in order of increasing gap.

We point out here that if $\tilde{\delta} \ll 1$, then the scales on which the GAIM scaling spectrum falls onto that of the normal metallic AIM can be essentially small; indeed one would expect that for $\tilde{\delta} \ll 1$ the scaling spectrum of the GAIM should approach that of the metallic case for frequencies around $\tilde{\omega} \sim 1$ at least, and hence one would still expect to see a partial Kondo resonance in the GAIM spectrum. That this is indeed the case will now be shown from the full scaling spectrum equation (39) for a range of increasing $\tilde{\delta}$.

5.2 Scaling spectra

In Figure 3(a) we show the LMA scaling spectrum, $\pi\Delta_0 D(\omega)$ versus $\tilde{\omega} = \omega/\omega_{\rm m}^0$, for $\tilde{\delta} = \delta/\omega_{\rm m}^0 = 0.01$ and 0.2 (solid lines, top to bottom), as well as for the metallic AIM, $\tilde{\delta} = 0$ (dotted line). Note first that, in agreement

with the preceding arguments, the GAIM spectra indeed coincide with those of the metallic AIM when $|\tilde{\omega}|$ is much greater than any of the chosen gaps $\tilde{\delta}$ (in practice for $|\tilde{\omega}| \gtrsim 4$). For the smallest gap shown, $\tilde{\delta} = 0.01$, the scaling spectrum coincides with the $\tilde{\delta} = 0$ spectrum down to frequency scales $\tilde{\omega} \sim \mathcal{O}(\tilde{\delta})$. The Kondo resonance of the metallic AIM is in consequence preserved more-or-less in its entirety when such a small gap is introduced; and even for the $\tilde{\delta} = 0.2$ example shown, a significant portion of the Kondo resonance remains intact. [We add that the small spectral 'glitches' at $\tilde{\omega} = 1 + \tilde{\delta}$ are a well known artifact of the RPA approximation used within the LMA self-energy [14,16]. They can be eliminated simply [16] by introducing a finite width $\propto \omega_{\rm m}$ to the resonance in $\mathrm{Im}\, \Pi^{+-}(\omega)$, although we shall not do so here—one gains only a very small correction to the spectrum (that can easily be deduced from the spectra in figure 3 just by smoothing out the artifacts 'by eye').]

Figure 3(b) shows LMA scaling spectra for larger gaps, $\tilde{\delta} = 0.5$, 2 and 5 (solid lines, in order of increasing spectral gap). Again the GAIM shows the same tails of the Kondo resonance as the metallic AIM, although now it is clear that for such large gap scales the main Kondo resonance itself is essentially lost.

Next we consider the bound states inside the gap. Figure 4(a) shows (solid line) the pole position $|\tilde{\omega}_{\rm p}| = \tilde{\omega}_{\rm p}/\omega_{\rm m}^0$ versus $\tilde{\delta}$ over a wide range of increasing gaps encompassing $\tilde{\delta} \ll 1$ to $\tilde{\delta} \gg 1$. The dotted lines show the asymptotic behaviour as $\tilde{\delta} \to 0$ [given by Eq. (45)], and as $\tilde{\delta} \to \infty$ (which is easily shown from Eq. (43) to be $|\omega_{\rm p}| = \delta$). The asymptotic forms are in fact seen to be applicable over the majority of the range of $\tilde{\delta}$, with substantial deviations occurring only for $\tilde{\delta} \sim 1$. In particular, the low-$\tilde{\delta}$ asymptote $|\omega_{\rm p}| = 2\tilde{\delta}^2$ (predicted also by NRG, as discussed in Sect. 3) holds for all gaps up to $\tilde{\delta} \sim 0.1$. Figure 4(b) shows the pole position $|\omega_{\rm p}|$ as a function of $\tilde{\delta}$, but now rescaled in terms of the gap as $|\omega_{\rm p}|/\delta$ (such that $|\omega_{\rm p}|/\delta < 1$ for poles in the gap). The figure shows more clearly the rather rapid crossover in the pole position $|\omega_{\rm p}|$, from the situation arising for small $\tilde{\delta}$ where the two symmetrically-disposed poles lie close to $\omega = 0$, to the large-$\tilde{\delta}$ behaviour where the poles approach the edges of the gap.

6 Numerical results at finite $\tilde{U}$

Now we present a survey of the numerics for finite $\tilde{U}$. These allow us to determine properties of the system which are inaccessible to analytic methods, such as the phase boundary between the GFL and LM phases. We study these in detail, and show that they compare very well to the predictions of NRG in Section 3. Second, the numerics for large-$\tilde{U}$ can be used to verify the asymptotic $\tilde{U} \gg 1$ results of Section 5.

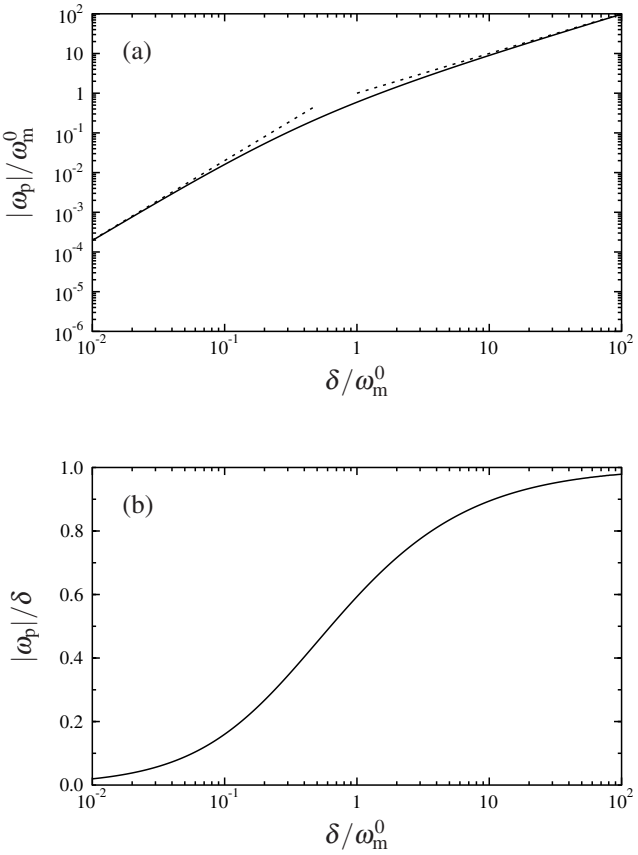

Fig. 4. (a) Position of the poles in the scaling spectrum, $|\omega_{\rm p}|/\omega_{\rm m}^0$ versus $\tilde{\delta} = \delta/\omega_{\rm m}^0$. The solid line is the result obtained from equation (43), whereas the dotted lines are the low- and high-$\tilde{\delta}$ asymptotes discussed in the text. (b) $|\omega_{\rm p}|/\delta$ versus $\tilde{\delta}$.

6.1 Phase boundaries

The LMA phase boundary is obtained as discussed in Section 4.1, and is shown in Figure 5 in the $(\delta/\omega_{\rm m}^0(\eta),\ \eta)$ plane for three different interaction strengths, $\tilde{U} = U/\pi\Delta_0 = 5$, 6 and 7 (solid lines from top to bottom).

It is seen directly from the figure that the LMA captures correctly the basic form of the phase boundary discussed in Section 3: there is a critical $\delta_{\rm c}$ for any asymmetry $\eta \neq 0$, below which the system is a GFL (singlet) phase and above which it is an LM doublet. For $\eta = 0$, *i.e.* precisely at particle-hole symmetry, the LM phase prevails for all $\delta > 0$.

Figure 5 also shows the phase boundary obtained from the effective low-energy model $H_{\rm eff}$ deduced from the NRG study of reference [11] (Eq. (11) above). $H_{\rm eff}/T_{\rm K}^0$ depends solely on K_0/D and $\alpha\sqrt{\delta/T_{\rm K}^0}$ (with α a coefficient of proportionality). For given $\tilde{U}$ and η $(= 1 + 2\epsilon_{\rm i}/U)$, the corresponding value of K_0/D may be obtained directly from a Schrieffer-Wolff transformation; and exact diagonalization of equation (11) then enables direct determination of the critical value of $\alpha\sqrt{\delta/T_{\rm K}^0}$ separating the GFL and LM phases. To compare to the LMA phase boundary (noting

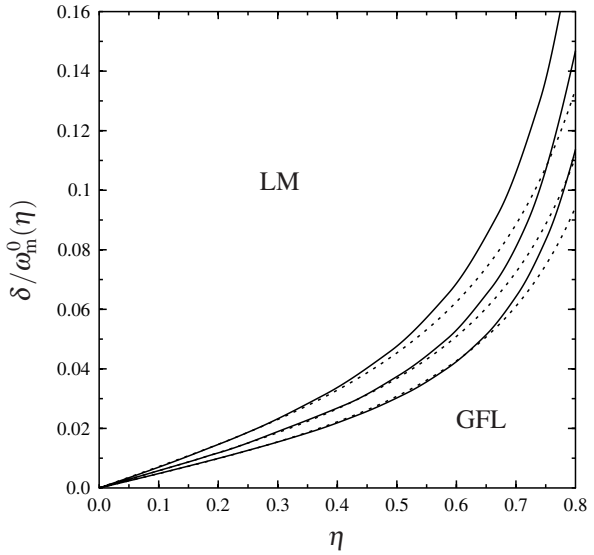

Fig. 5. Evolution of the LMA phase boundary in the $(\delta/\omega_{\rm m}^0(\eta),\ \eta)$ plane, with increasing interaction strength $\tilde{U}$. The solid lines from top to bottom are the phase boundaries for $\tilde{U} = 5$, 6 and 7; the dotted lines show comparison to the asymptotic result [11] (see text).

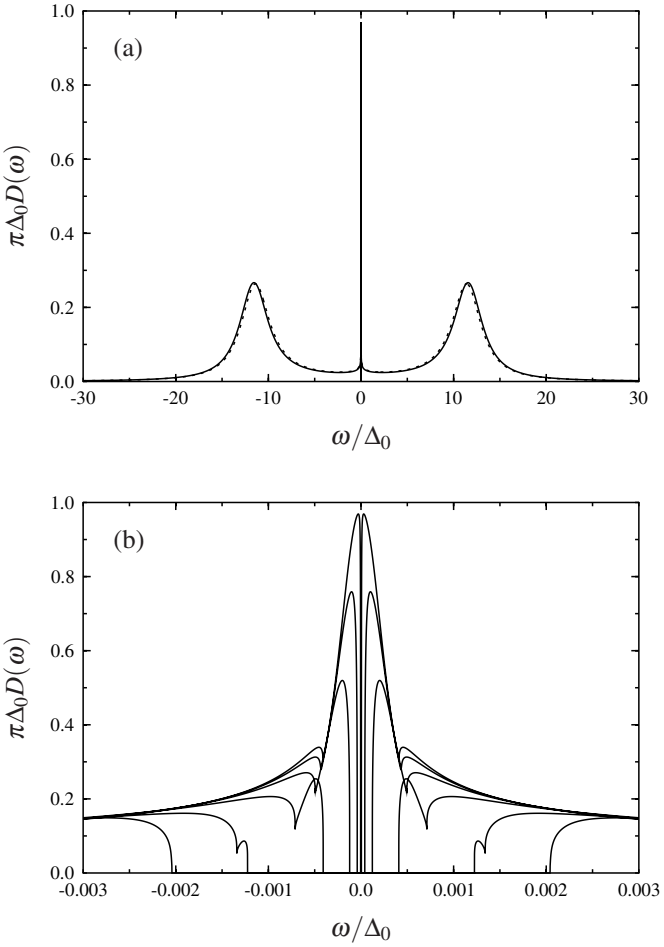

Fig. 6. LMA single-particle spectra, $\pi\Delta_0 D(\omega)$ *vs.* ω/Δ_0, for fixed $\tilde{U} = 7$ at particle-hole symmetry ($\eta = 0$). (a) Spectra on all energy scales, for $\delta/\omega_{\rm m}^0 = 0.01$ (solid line) and 5 (dotted line). (b) Spectra on low energy scales, for $\delta/\omega_{\rm m}^0 = 0.01$, 0.1, 0.3, 1, 3 and 5.

that $\omega_{\rm m}^0 \propto T_{\rm K}^0$), for given $\tilde{U}$ the constant α is simply chosen to fit the resultant phase boundary of the effective model to our LMA result at a single $\eta = 0.2$ (and we add further that the resultant $\alpha \sim \mathcal{O}(1)$ is constant to $\lesssim 3\%$ as $\tilde{U}$ is varied over the range shown in Fig. 5).

The primary point from Figure 5 is that there is clearly excellent agreement between the LMA phase boundary and the asymptotic result [11], particularly for small η. It is also clear that the agreement becomes better at larger values of η upon increasing $\tilde{U}$. The latter observation is readily explained. First, the NRG result calculated from equation (11) applies to the gapped *Kondo* model. Although the GAIM maps to the Kondo model via the Schrieffer-Wolff transformation [2], this mapping holds asymptotically for $\tilde{U} \gg 1$ and $\tilde{\epsilon}_{\rm i} \ll -1$, hence from equation (10) requires $\frac{1}{2}U(1-\eta) \gg 1$, and is not therefore applicable as η tends to 1 (where mixed-valent behaviour arises). Second, $H_{\rm eff}$ (Eq. (11)) by definition applies in the limit $\delta/T_{\rm K}^0 \ll 1$ [see the discussion preceding Eq. (11)]. Since $\delta_{\rm c}/\omega_{\rm m}^0$ ($\propto \delta_{\rm c}/T_{\rm K}^0$) increases rapidly as η increases, equation (11) is inapplicable even to the Kondo model at larger η.

6.2 Particle-hole–symmetric limit

We now examine the behaviour in each of the two phases; starting with the simplest case of particle-hole–symmetry.

Figure 6 shows the evolution of the single-particle spectrum, $\pi\Delta_0 D(\omega)$ *vs.* ω/Δ_0, as the gap is increased at a fixed $\tilde{U} = 7$. Figure 6(a) shows the spectra for gaps $\delta/\omega_{\rm m} = 0.01 \ll 1$ and 5 (solid and dotted lines, respectively). On this 'all scales' level the spectra are dominated by the Hubbard satellite peaks, centred on $\omega \sim \pm U/2$ and with HWHM $\sim 2\Delta_0$ (the satellites arise also at the level of static mean-field theory, although [14] UHF underestimates their width by a factor of 2 because it neglects the low-energy inelastic scattering processes that are included within the LMA). Figure 6 shows clearly that the high-energy spectral features are essentially unchanged by varying the gap on the scale of $\omega_{\rm m}^0$—as expected from scaling arguments—and as such we shall not consider them further.

Figure 6(b) shows the more complex behaviour that occurs on the scale of the gap itself, showing the low-frequency spectrum for $\delta/\omega_{\rm m}^0 = 0.01$, 0.1, 0.3, 1, 3 and 5 (for clarity only the continuum parts of the spectra are shown—the poles are discussed below). As for the $\tilde{U} \gg 1$ asymptotics of Section 5, we see that the finite-$\tilde{U}$ LMA captures the basic result known from NRG: that the physics of the problem on energy scales much greater than the gap is virtually unchanged from that of the gapless limit. For very small gaps in comparison to $\omega_{\rm m}^0$, the

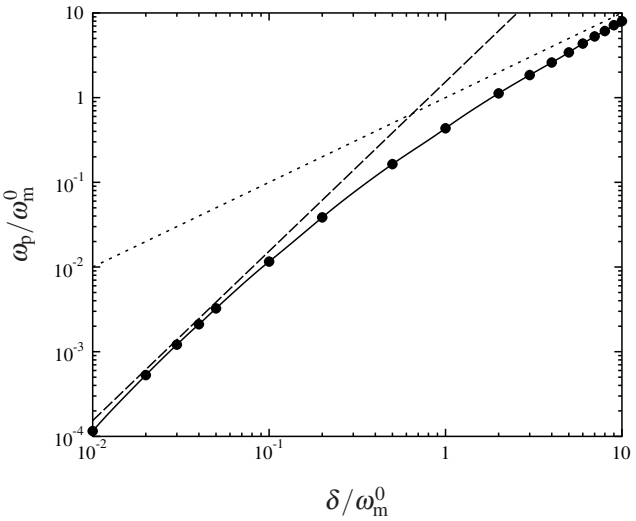

Fig. 7. Evolution of the pole positions in the single-particle spectrum, ω_p/ω_m^0 *vs.* δ/ω_m^0, for $\tilde{U} = 7$ at particle-hole symmetry. The circles are the full numerical results, while the dotted and dashed lines are asymptotes discussed in the text.

spectra show the characteristic Kondo resonance associated with the local Fermi liquid behaviour of the metallic Anderson model at $\omega \sim \omega_m^0$; only on much lower frequency scales is the true, non–Fermi-liquid LM behaviour (characterized by two poles inside the gap) revealed. As δ increases in Figure 6(b), the Kondo resonance arising for $\delta = 0$ is gradually destroyed from the inside, and the corresponding spectral weight is reassigned to the poles in the gap. Even when the resonance is completely eliminated though, remnants of Kondo physics remain in the slow logarithmic tails of the erstwhile resonance, which persist up to non-universal frequency scales on the order of Δ_0.

We now consider the poles inside the gap, arising at frequencies $\omega = \pm\omega_p$, with ω_p given from equation (16) and equation (3) by solution of

$$\omega_p - \epsilon_i - \Delta_R(\omega_p) - \tilde{\Sigma}_\downarrow^R(\omega_p) = 0. \qquad (47)$$

Figure 7 shows ω_p/ω_m^0 as a function of the gap δ/ω_m^0, for $\tilde{U} = 7$ as considered above. The circles show the points obtained by full numerical calculation (the solid line is a guide to the eye). The dotted line marks the extent of the gap, δ/ω_m, and the dashed line is the approximation

$$\frac{\omega_p}{\omega_m^0} \sim 2\left(1 - \frac{16\Delta_0}{\pi U}\right)\left(\frac{\delta}{\omega_m^0}\right)^2, \qquad (48)$$

which is readily obtained in the same manner as the $\tilde{U} \gg 1$ analysis of Section 5.1 [which gives the result Eq. (45)] but with the leading $\mathcal{O}(1/\tilde{U})$ correction to ω_m/ω_m^0 in equation (A-10) retained.

In Section 5.1 we showed that the single-particle spectrum in the strong coupling limit $\tilde{U} \gg 1$ is a universal function of ω/ω_m^0 for given δ/ω_m^0, and obtained the scaling spectrum analytically (Eq. (39)). Here we test this result by direct comparison to numerical calculations at finite $\tilde{U}$. Since $D(\omega)$ is a universal function of ω/ω_m^0, the numerical spectra should collapse onto the analytic result for sufficiently large $\tilde{U}$.

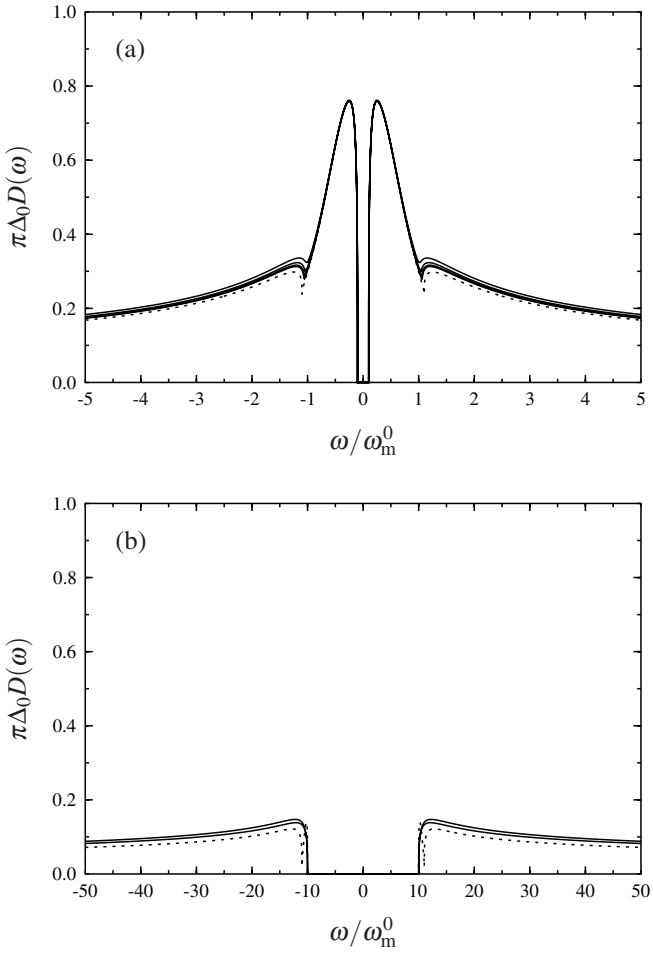

Fig. 8. LMA scaling spectra in the particle-hole–symmetric limit. $\pi\Delta_0 D(\omega)$ *vs.* ω/ω_m^0 for (a) fixed $\delta/\omega_m^0 = 0.1$ and $\tilde{U} = 4$, 5, 6 and 7, and (b) fixed $\delta/\omega_m^0 = 10$ with $\tilde{U} = 5$ and 7 (solid lines, top to bottom). In both figures the dotted line is the corresponding analytic result equation (39).

Figure 8(a) illustrates this behaviour for fixed δ/ω_m^0=0.1: the solid lines from top to bottom are the numerical LMA spectra for $\tilde{U} = 4$, 5, 6 and 7, while the dotted line is the asymptotic $\tilde{U} \gg 1$ result, equation (39). As seen in the figure, the spectral collapse discussed above is apparent; the agreement becomes progressively better as $\tilde{U}$ increases as one would expect, and the $\tilde{U} \gg 1$ result is a very good approximation to the true spectrum for values of $\tilde{U}$ as low as 5 or so. A similar comparison is given in Figure 8(b), this time for a much larger gap, $\delta/\omega_m^0 = 10$. The solid lines are the numerical spectra for $\tilde{U} = 5$ and $\tilde{U} = 7$ (from top to bottom) while the dotted line is the $\tilde{U} \gg 1$ result; the agreement is again good.

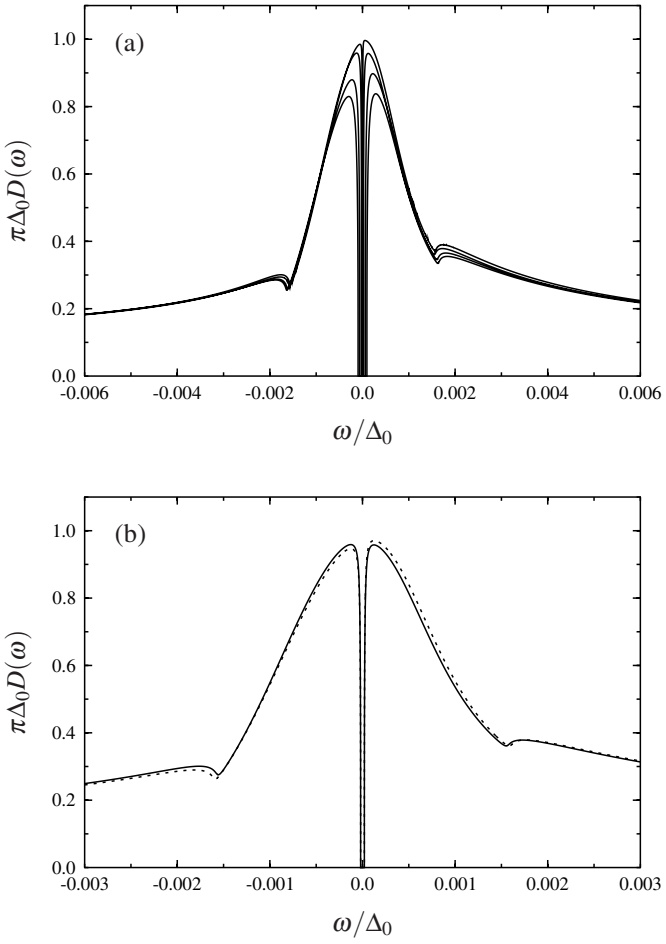

Fig. 9. Single-particle spectra away from particle-hole symmetry. (a) $\pi\Delta_0 D(\omega)$ *vs.* ω/Δ_0 for $\tilde{U} = 6$, $\eta = 0.22$ and $\delta/\Delta_0 = 4.00\times10^{-6}$, 1.989×10^{-5}, 3.58×10^{-5} and 9.54×10^{-5} (in order of increasing gap in the figure). (b) Spectra on either side of $\delta_c \simeq 1.99\times10^{-5}\Delta_0$ for the same $\tilde{U}$ and η: the solid line is for δ_c^-, the dotted for δ_c^+.

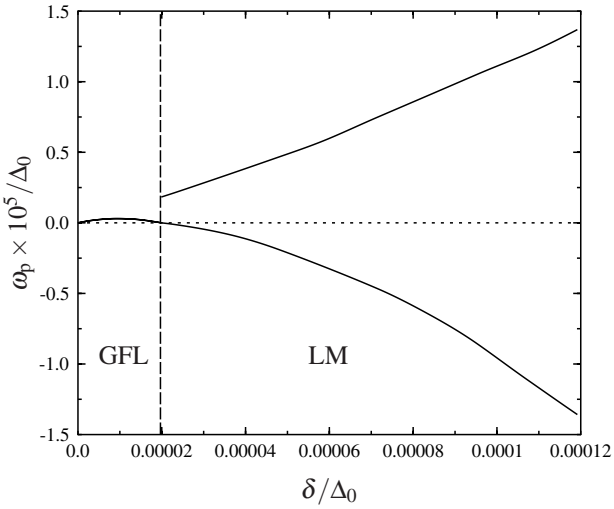

Fig. 10. Pole positions in the single-particle spectrum $D(\omega)$: ω_p/Δ_0 *vs.* δ/Δ_0, for $\tilde{U} = 6$ and $\eta = 0.22$. The dashed line marks the phase boundary at $\delta_c \simeq 1.99\times10^{-5}\Delta_0$.

6.3 Away from particle-hole symmetry

We now consider briefly results for dynamics away from particle-hole symmetry, as the system evolves from the GFL to the LM phase with increasing gap, δ. For illustration we consider an asymmetry $\eta = 1 + 2\epsilon_i/U = 0.22$ and $\tilde{U} = 6$, for which (from the method of Sect. 4.2.2) the critical gap for the GFL↔LM transition is found to be $\delta_c/\Delta_0 \simeq 1.99\times10^{-5}$.

The evolution of the continuum part of the single-particle spectrum across the phase boundary is shown in Figure 9(a), for gaps $\delta/\Delta_0 = 4.00\times10^{-6}$, 1.989×10^{-5}, 3.58×10^{-5} and 9.54×10^{-5}; *i.e.* for $\delta/\delta_c \simeq 0.2, 0.999, 1.8$ and 4.8, the smallest gap thus corresponding to a point 'deep' in the GFL phase, the next to a point just inside the GFL phase, and the other two to points inside the LM phase. But since all four gaps are much smaller than the Kondo scale in the absence of the gap, $\omega_m^0/\Delta_0 \approx 1.6\times10^{-3}$, all the spectra show residual Kondo resonances for $\omega \gtrsim \delta$ and collapse onto the common tails occurring in the gapless case $\delta = 0$ [15] when $\omega \gg \delta$. That this behaviour is correct follows from the discussion at the end of Section 3, and indicates that the LMA captures the correct $\omega \gg \delta$ physics of the problem in both GFL and LM phases away from particle-hole symmetry.

Figure 9(b) shows the spectra just on either side of the phase boundary, the solid line for $\delta = \delta_c^-$ (GFL phase), and the dotted line for $\delta = \delta_c^+$ (LM phase). There is a slight discontinuity in the spectrum across the phase transition, not unexpectedly: the NRG effective Hamiltonian [11] considered in Section 3 implies that the level-crossing phase transition is discontinuous, such that different low-energy many-body excited states are accessible from the GFL and LM ground states (see Fig. 1).

Considering now the bound states in the spectral gap, Figure 10 shows the pole positions in the single-particle spectrum ω_p/Δ_0 *vs.* the gap δ/Δ_0. In the GFL phase a single pole occurs in the gap (here occurring at $\omega_p > 0$); while in the LM phase for $\delta > \delta_c$ two distinct poles arise, one either side of the Fermi level $\omega = 0$, such that the higher energy excitation emerges discontinuously at $\delta = \delta_c^+$ on crossing into the LM phase. This behaviour is of course precisely that arising from the effective NRG Hamiltonian equation (11), the low-lying states of which are illustrated schematically in Figure 1 and in terms of which the poles in Figure 10 can be interpreted directly: in the GFL phase $\delta < \delta_c$, the single pole in $D(\omega)$ for $\omega_p > 0$—corresponding as such to the addition of an electron—arises from the $(-1,0) \to (0,\frac{1}{2})$ transition of the effective low-energy model equation (11); in the LM phase by contrast, the pole at $\omega_p < 0$ corresponds to the transition between the same two levels but in the opposite direction [since $(0,\frac{1}{2})$ is now the ground state], whereas the pole arising at a finite, positive frequency as soon as one enters the LM phase corresponds to the $(0,\frac{1}{2}) \to (1,0)$ transition of Figure 1. Hence the LMA indeed recovers

the low-energy physics expected away from particle-hole symmetry.

Finally, the essential effect of increasing the gap further is as seen previously for the particle-hole–symmetric limit (*cf.* Fig. 6). As $\delta/\omega_{\rm m}^0$ increases, what remains of the Kondo resonance is gradually destroyed from within until the central resonance itself is destroyed, although the tails of the resonance persist for $\omega \gg \delta$ and do so until δ is of the order of the non-universal scale Δ_0. At lower frequencies, the pole structure continues the trend observed in Figure 10, with the two poles in the LM phase spectrum moving slowly outwards toward the edges of the gap as δ is increased.

7 Single self-energy

Throughout the paper we have focused naturally on the two–self-energy energy description that is central to the LMA, with associated self-energies $\tilde{\Sigma}_\sigma(\omega)$ (as in Eq. (14)) which determine the local propagator $G(\omega)$ via equation (13). Once $G(\omega)$ is known, the conventional single–self-energy $\Sigma(\omega)$ (which, like $G(\omega)$, is independent of spin in the absence of an applied magnetic field) can of course be obtained as a byproduct: either from its definition via the Dyson equation $G(\omega) = [g(\omega)^{-1} - \Sigma(\omega)]^{-1}$ (Eq. (8), with $g(\omega)$ the non-interacting propagator Eq. (3)), or equivalently upon comparison of equation (8) and equation (13) which yields [15]

$$\Sigma(\omega) = \tfrac{1}{2}[\tilde{\Sigma}_\uparrow(\omega) + \tilde{\Sigma}_\downarrow(\omega)] + \frac{[\frac{1}{2}(\tilde{\Sigma}_\uparrow(\omega) - \tilde{\Sigma}_\downarrow(\omega))]^2}{g(\omega)^{-1} - \frac{1}{2}[\tilde{\Sigma}_\uparrow(\omega) + \tilde{\Sigma}_\downarrow(\omega)]}, \tag{49}$$

and hence enables $\Sigma(\omega)$ $(= \Sigma^{\rm R}(\omega) - {\rm isgn}(\omega)\Sigma^{\rm I}(\omega))$ to be determined directly from the $\{\tilde{\Sigma}_\sigma(\omega)\}$. We now comment briefly on the analytic behaviour of $\Sigma(\omega)$ that is characteristic of both of the GFL and LM phases, at low-frequencies inside the gap where $G(\omega)^{-1} \equiv [\omega - \epsilon_{\rm i} - \Delta_{\rm R}(\omega) - \Sigma^{\rm R}(\omega)] + {\rm isgn}(\omega)[0^+ + \Sigma^{\rm I}(\omega)]$ (the imaginary part of the hybridization function vanishing inside the gap).

First we show that analyticity alone implies that if $\Sigma(\omega)$ contains $n \geq 0$ poles inside the gap, then $G(\omega)$ contains $n+1$ poles in the gap. To see this, note that $\Sigma^{\rm I}(\omega) \geq 0\ \forall\omega$, and separate $\Sigma^{\rm I}(\omega) = \Sigma^{\rm I}_{\rm band}(\omega) + \Sigma^{\rm I}_{\rm pole}(\omega)$ where the 'band' piece $\Sigma^{\rm I}_{\rm band}(\omega) \geq 0$ is non-vanishing only outside the gap $|\omega| > \delta$, while $\Sigma^{\rm I}_{\rm pole}(\omega)$ denotes any contributions from poles inside the gap. From Hilbert transformation it follows directly that the real part $\Sigma^{\rm R}_{\rm band}(\omega)$ is a monotonically decreasing function of ω inside the gap; whence from equation (7) $\Delta_{\rm R}(\omega) + \Sigma^{\rm R}_{\rm band}(\omega)$ is monotonically decreasing inside the gap, from $+\infty$ at $\omega = -\delta$ to $-\infty$ at $\omega = +\delta$. Now consider the case $n = 0$ where there are no poles in $\Sigma(\omega)$ inside the gap, $\Sigma^{\rm I}(\omega) = 0$ for all $|\omega| < \delta$; such that $\Delta_{\rm R}(\omega) + \Sigma^{\rm R}(\omega) \equiv \Delta_{\rm R}(\omega) + \Sigma^{\rm R}_{\rm band}(\omega)$ thus decreases monotonically with ω, from $+\infty$ at $\omega = -\delta$ to $-\infty$ at $\omega = +\delta$. In consequence, $\omega - \epsilon_{\rm i} - [\Delta_{\rm R}(\omega) + \Sigma^{\rm R}(\omega)]$ is guaranteed to vanish once only inside the gap; and hence $G(\omega)$ contains a single pole inside the gap. For the case $n = 1$ where $\Sigma(\omega)$ contains a single pole inside the gap (say at $\omega = \omega_1$), $\Delta_{\rm R}(\omega) + \Sigma^{\rm R}(\omega) \equiv \Delta_{\rm R}(\omega) + \Sigma^{\rm R}_{\rm band}(\omega) + \Sigma^{\rm R}_{\rm pole}(\omega)$, and it is elementary to show that $\Delta_{\rm R}(\omega) + \Sigma^{\rm R}(\omega)$ is now a monotonically decreasing function of ω in the *two* intervals $-\delta < \omega < \omega_1$ and $\omega_1 < \omega < +\delta$; ranging from $+\infty$ at the lower end of each interval to $-\infty$ at the upper end of each interval. Hence $\omega - \epsilon_{\rm i} - [\Delta_{\rm R}(\omega) + \Sigma^{\rm R}(\omega)]$ vanishes once and only once in *each* interval; and $G(\omega)$ thus contains two poles. Extension of the argument to arbitrary n is direct.

The behaviour of $\Sigma(\omega)$ in the GFL phase is quite simple, since as found in the preceding sections $G(\omega)$ obtained from the LMA has a single pole inside the gap. In consequence, from the argument above, $\Sigma(\omega)$ does not have a pole inside the gap; and we note that this behaviour is precisely that required from perturbation theory in U to all orders à la Luttinger (as shown in [13]), reflecting as such the adiabatic continuity to the non-interacting limit that is characteristic of the GFL phase.

The LM phase by contrast is more subtle. In this case we know as above that $G(\omega)$ has *two* poles inside the gap, one on either side of the Fermi level. Hence $\Sigma(\omega)$ has a single pole inside the gap. This behaviour is apparent from equation (49), noting that the $\tilde{\Sigma}^{\rm I}_\sigma(\omega)$ vanish throughout the gap (for both $\sigma = \uparrow$ and $\downarrow$). This is particularly straightforward to show in the particle-hole symmetric case, where by symmetry $\tilde{\Sigma}^{\rm R}_\downarrow(-\omega) = U - \tilde{\Sigma}^{\rm R}_\uparrow(\omega)$ [15]; and in consequence $\frac{1}{2}[\tilde{\Sigma}^{\rm R}_\uparrow(\omega = 0) + \tilde{\Sigma}^{\rm R}_\downarrow(\omega = 0)] = U/2$ $(\equiv -\epsilon_{\rm i})$ – whence the denominator in equation (49) vanishes as $\omega \to 0$, while the (pure real) numerator remains finite because symmetry is not restored and hence $\tilde{\Sigma}^{\rm R}_\uparrow(\omega = 0) \neq \tilde{\Sigma}^{\rm R}_\downarrow(\omega = 0)$. The single–self-energy $\Sigma(\omega)$ thus indeed has a pole, and it lies precisely at the Fermi level: $\Sigma(\omega) \propto 1/\omega^+$, which is the behaviour one expects from perturbative continuity to the *atomic* limit of vanishing hybridization [13] (as is physically natural for a LM phase). Away from particle-hole symmetry, the single pole in $\Sigma(\omega)$ inside the gap now lies at a non-zero frequency, which is readily shown from equation (49) to occur when $g(\omega)^{-1} = \frac{1}{2}[\tilde{\Sigma}^{\rm R}_\uparrow(\omega) + \tilde{\Sigma}^{\rm R}_\downarrow(\omega)]$. And on crossing the transition from the GFL phase to the LM phase, the pole in $\Sigma(\omega)$ at $\omega \neq 0$ arises abruptly; precisely as required from the general considerations of Section 3.

8 Conclusion

In this paper we have extended the local moment approach to the gapped AIM. The two-self–energy description and the self-energy diagrams used in the present approach are naturally the same as those used in previous LMA studies, but the precise forms of the self-energies depend crucially upon the underlying mean-field parameters ($|\mu|$ and $e_{\rm i}$), the determination of which is very different in the case of the GAIM.

We explained how symmetry restoration, in combination with the generalized Friedel sum rule appropriate to the GAIM [13], can be used to handle the GFL phase. In the LM phase by contrast, we used simple arguments to show how the mean-field parameters must be chosen to

recover the physics of the problem. We then analysed the particle-hole–symmetric limit of the model analytically, obtaining universal single-particle scaling spectra for the model. In addition, the low-frequency bound state (pole) behaviour of these spectra (for gaps δ small in comparison to the Kondo scale) was found to be of precisely the form expected from NRG [11].

A brief survey of numerical results followed. The phase boundary between the GFL and LM phases was compared to predictions from the NRG, and found to be in quantitative agreement over the range of parameters for which such a comparison is appropriate. Analysis of the particle-hole–symmetric limit at finite-U/Δ_0 was found to confirm the asymptotic strong coupling behaviour predicted in Section 5, while away from particle-hole–symmetry we analyzed the behaviour of the system on both sides of the phase boundary, showing how our approach indeed captures the discontinuous nature of the transition in a non-trivial fashion.

We are grateful to the EPSRC for financial support, via Grant No. EP/D050952/1.

Appendix A: strong coupling analytic results at particle-hole symmetry

Here we outline in particular the derivation of equation (36) and equation (37) appropriate to the strong coupling ($\tilde{U} = U/\pi\Delta_0 \gg 1$) behaviour of the GAIM at particle-hole symmetry; with the gap δ taken to be any finite multiple of the low-energy Kondo scale in the absence of the gap, $\omega_{\rm m}^0$.

A.1 Strong-coupling asymptotics of $\omega_{\rm m}(\delta)$

We begin by deriving an expression for the low-energy scale $\omega_{\rm m} \equiv \omega_{\rm m}(\delta)$ (which will be used in Appendix A.2 below). Our starting point is a result obtained originally for the metallic AIM [14], where it is shown analytically that the position of the resonance in $\mathrm{Im}\,\Pi^{+-}(\omega)$ (*i.e.* $\omega_{\rm m}^0 = \omega_{\rm m}(\delta = 0)$) is related to the local moment $|\mu|$ by

$$|\mu| \overset{\tilde{U}\gg 1}{\sim} |\mu_0| + \frac{\omega_{\rm m}^0}{U} \quad : \quad \delta = 0. \tag{A-1}$$

Numerically we find it this relation holds also for the gapped AIM (provided $\delta/\Delta_0 \ll 1$, as relevant here), *viz.*

$$|\mu(\delta)| \overset{\tilde{U}\gg 1}{\sim} |\mu_0(\delta)| + \frac{\omega_{\rm m}(\delta)}{U}. \tag{A-2}$$

Therefore

$$\omega_{\rm m}(\delta) \sim U\Big[|\mu(\delta)| - |\mu_0(\delta)|\Big], \tag{A-3}$$

and in the $\delta = 0$ limit in particular,

$$\omega_{\rm m}^0 \equiv \omega_{\rm m}(0) \sim U\Big[|\mu(0)| - |\mu_0(0)|\Big]. \tag{A-4}$$

As discussed in Section 4.2.1, $|\mu(\delta)| = |\mu(0)|$ when the gap is sufficiently small, and hence we can eliminate $|\mu(\delta)|$ and $|\mu(0)|$ from equation (A-3) and equation (A-4) to obtain

$$\omega_{\rm m}(\delta) \sim \omega_{\rm m}^0 - U\Big[|\mu_0(\delta)| - |\mu_0(0)|\Big]. \tag{A-5}$$

This result expresses the δ-dependence of the LMA $\omega_{\rm m}(\delta)$ in terms of that of the UHF moment $|\mu_0(\delta)|$, which can in turn be calculated analytically from the form of the UHF spectrum, equation (18), alone. Obtaining this asymptotic behaviour of $|\mu_0(\delta)|$ is somewhat lengthy, but in strong-coupling $\tilde{U} \gg 1$ the result is

$$|\mu_0(\delta)| - |\mu_0(0)| \sim \frac{8\Delta_0\delta}{\pi U^2}\left[1 - \frac{8\Delta_0}{\pi U}\ln\left(\frac{4\delta}{U}\right)\right], \tag{A-6}$$

whence equation (A-5) gives

$$\omega_{\rm m}(\delta) - \omega_{\rm m}^0 \sim -\frac{8\Delta_0\delta}{\pi U}\left\{1 - \frac{8\Delta_0}{\pi U}\left[\ln\left(\frac{4\delta}{\omega_{\rm m}^0}\right) + \ln\left(\frac{\omega_{\rm m}^0}{U}\right)\right]\right\}. \tag{A-7}$$

Since the LMA for the metallic AIM [14] gives

$$\omega_{\rm m}^0 = \beta U \exp\left(\frac{-\pi U}{8\Delta_0}\right) \tag{A-8}$$

with β a pure constant $\mathcal{O}(1)$, it follows that

$$\omega_{\rm m}(\delta) - \omega_{\rm m}^0 \sim -\frac{8\Delta_0\delta}{\pi U}\left\{2 - \frac{8\Delta_0}{\pi U}\left[\ln\left(\frac{4\delta}{\omega_{\rm m}^0}\right) + \ln\beta\right]\right\}. \tag{A-9}$$

Hence to leading order in Δ_0/U, the behaviour of the low-energy scale of the GAIM is

$$\frac{\omega_{\rm m}(\delta)}{\omega_{\rm m}^0} \sim 1 - \frac{16\Delta_0}{\pi U}\frac{\delta}{\omega_{\rm m}^0}, \tag{A-10}$$

(where it is implicitly understood that for $\delta > \pi U\omega_{\rm m}^0/(16\Delta_0)$, the scale $\omega_{\rm m}(\delta)$ remains at zero according to Fig. 2).

A.2 Strong-coupling behaviour of the single-particle spectrum

We now outline how the asymptotic strong-coupling behaviour of the LMA self-energies can be obtained. Once these are known, the spectrum $D(\omega)$ follows in closed form as considered in Section 5.

We begin by considering the form of $\mathrm{Im}\,\Pi^{+-}(\omega)$ in strong-coupling. As mentioned briefly in Section 4, the dominant excitation in $\mathrm{Im}\,\Pi^{+-}(\omega)$ for finite $\tilde{U}$ is either a pole or a resonance centred on $\omega = \omega_{\rm m}$, depending on the size of δ. In strong coupling $\tilde{U} \gg 1$ however, as for the case of the metallic AIM [14], the sharp resonance in $\mathrm{Im}\,\Pi^{+-}(\omega)$ tends asymptotically to a pole; all its weight lies at a frequency $\omega_{\rm m} > 0$, and it is normalized according to [14]

$$\frac{1}{\pi}\int_0^\infty \mathrm{d}\omega\ \mathrm{Im}\,\Pi^{+-}(\omega) \overset{\tilde{U}\gg 1}{\sim} 1. \tag{A-11}$$

Hence we write

$$\mathrm{Im}\,\Pi^{+-}(\omega) = \pi\delta(\omega - \omega_{\mathrm{m}}). \tag{A-12}$$

By inserting this into the LMA dynamical self-energy $\Sigma_\uparrow(\omega)$ —which can be conveniently expressed as [14]

$$\Sigma_\uparrow(\omega) = \frac{U^2}{\pi}\int_{-\infty}^{\infty} \mathrm{d}\omega_1\, \mathrm{Im}\Pi^{+-}(\omega_1) \times \Big[\theta(\omega_1)\mathcal{G}_\downarrow^-(\omega_1+\omega) + \theta(-\omega_1)\mathcal{G}_\downarrow^+(\omega_1+\omega)\Big] \tag{A-13}$$

with

$$\mathcal{G}_\sigma^\pm(\omega) = \int_{-\infty}^{\infty} \mathrm{d}\omega_1\, \frac{D_\sigma^0(\omega_1)\theta(\pm\omega_1)}{\omega - \omega_1 \pm \mathrm{i}0^+} \tag{A-14}$$

—it is readily shown [16] that

$$\Sigma_\uparrow^{\mathrm{R}}(\omega) \overset{\tilde{U}\gg 1}{\sim} U^2\,\mathrm{Re}\,\mathcal{G}_\downarrow^-(\omega+\omega_{\mathrm{m}}). \tag{A-15}$$

The mean-field spectrum $D_\sigma^0(\omega)$ required to calculate $\mathrm{Re}\,\mathcal{G}_\downarrow^-(\omega)$ itself follows from equations (15) and (18) (with $e_{\mathrm{i}} = 0$ at particle-hole symmetry). In strong-coupling, $|\mu| \to 1$ and one obtains

$$D_\sigma^0(\omega) = {}^{b}D_\sigma^0(\omega) + Q_\sigma\delta(\omega - \omega_{\mathrm{p},\sigma}^0) \tag{A-16}$$

where the 'band' contribution to the spectrum, ${}^{b}D_\sigma^0(\omega)$ is

$${}^{b}D_\sigma^0(\omega) = \frac{\pi^{-1}\Delta_0\theta(|\omega|-\delta)}{[\omega + \frac{1}{2}\sigma U - \Delta_{\mathrm{R}}(\omega)]^2 + \Delta_0^2} \tag{A-17}$$

and the pole position is given by

$$\omega_{\mathrm{p},\sigma}^0 + \tfrac{1}{2}\sigma U = \Delta_{\mathrm{R}}(\omega_{\mathrm{p},\sigma}^0). \tag{A-18}$$

For $D_\downarrow^0(\omega)$ in particular it is readily shown that the pole lies at a positive frequency; hence, inserting equation (A-16) into equation (A-14),

$$\mathrm{Re}\,\mathcal{G}_\downarrow^-(\omega+\omega_{\mathrm{m}}) = \int_{-\infty}^{-\delta} \mathrm{d}\omega_1\, {}^{b}D_\downarrow^0(\omega_1)\mathrm{P}\left(\frac{1}{\omega+\omega_{\mathrm{m}}-\omega_1}\right). \tag{A-19}$$

(where we use the fact that ${}^{b}D_\downarrow^0(\omega)$ in equation (A-17) has no weight for $|\omega| < \delta$ to replace the upper limit of the integral in equation (A-14) by $-\delta$). This integral is dominated by its logarithmic singularity; and since $D_\downarrow^0(\omega) \sim 4\Delta_0/(\pi U^2)$ is a slowly-varying function of ω when $\delta < |\omega| \ll U$ we can write [14]

$$\mathrm{Re}\,\mathcal{G}_\downarrow^-(\omega) \sim \frac{4\Delta_0}{\pi U^2}\int_{-U}^{-\delta} \mathrm{d}\omega_1\, \mathrm{P}\left(\frac{1}{\omega+\omega_{\mathrm{m}}-\omega_1}\right) \tag{A-20}$$

where we have replaced the lower limit in equation (A-19) by a high-energy cutoff of $-U$, as likewise employed for the metallic AIM [14,16] (and the precise value of the cutoff being immaterial [14,16]).

Performing the integration in equation (A-20) and substituting the result into equation (A-15), yields

$$\Sigma_\uparrow^{\mathrm{R}}(\omega) \sim -\frac{4\Delta_0}{\pi}\ln\left|\frac{\omega+\omega_{\mathrm{m}}+\delta}{U}\right| \tag{A-21}$$

(where $\omega + \omega_{\mathrm{m}} + U$ in the denominator of the logarithm has naturally been replaced by U). The full LMA result for $\epsilon_{\mathrm{i}} + \tilde{\Sigma}_\uparrow^{\mathrm{R}}(\omega)$ (with $\epsilon_{\mathrm{i}} = -U/2$ at particle-hole symmetry), including the static self-energy contribution $\tilde{\Sigma}_\uparrow^0$ from equation (16) (which vanishes asymptotically in strong coupling where $|\mu| \equiv 1$), then follows as

$$\epsilon_{\mathrm{i}} + \tilde{\Sigma}_\uparrow^{\mathrm{R}}(\omega) \sim -\frac{U}{2} - \frac{4\Delta_0}{\pi}\ln\left|\frac{\omega+\omega_{\mathrm{m}}+\delta}{U}\right|. \tag{A-22}$$

We now rewrite equation (A-22) in a more convenient form by noting that for the gapless AIM, $\delta = 0$, the symmetry restoration condition requires that $\epsilon_{\mathrm{i}} + \tilde{\Sigma}_\uparrow^{\mathrm{R}}(\omega = 0) = 0$ (as follows from Eq. (22) together with the general result that $\epsilon_{\mathrm{i}} + \tilde{\Sigma}_\uparrow^{\mathrm{R}}(\omega) = -[\epsilon_{\mathrm{i}} + \tilde{\Sigma}_\downarrow^{\mathrm{R}}(-\omega)]$ at particle-hole symmetry). Hence from equation (A-22) with $\delta = 0$,

$$\epsilon_{\mathrm{i}} + \tilde{\Sigma}_\uparrow^{\mathrm{R}}(\omega=0) \sim -\frac{U}{2} - \frac{4\Delta_0}{\pi}\ln\left|\frac{\omega_{\mathrm{m}}^0}{U}\right| = 0. \tag{A-23}$$

Subtracting equation (A-23) from equation (A-22) then gives

$$\epsilon_{\mathrm{i}} + \tilde{\Sigma}_\uparrow^{\mathrm{R}}(\omega) \sim -\frac{4\Delta_0}{\pi}\ln\left|\frac{\omega+\omega_{\mathrm{m}}+\delta}{\omega_{\mathrm{m}}^0}\right|. \tag{A-24}$$

Finally, we insert the explicit form of $\omega_{\mathrm{m}}(\delta)$ given by equation (A-10) into equation (A-24), to obtain the leading asymptotic behaviour

$$-\frac{U}{2} + \tilde{\Sigma}_\uparrow^{\mathrm{R}}(\omega) \overset{\tilde{U}\gg 1}{\sim} -\frac{4\Delta_0}{\pi}\ln\left(\tilde{\omega}+\tilde{\delta}+1\right) \tag{A-25}$$

where $\tilde{\omega} = \omega/\omega_{\mathrm{m}}^0$ and $\tilde{\delta} = \delta/\omega_{\mathrm{m}}^0$ (and we use $\tilde{\delta}(1-\frac{16}{\pi^2\tilde{U}}) \to \tilde{\delta}$ for $\tilde{U} \gg 1$).

The corresponding $\Sigma_\uparrow^{\mathrm{I}}(\omega) \equiv \tilde{\Sigma}_\uparrow^{\mathrm{I}}(\omega)$ follows likewise from equations (A-12)–(A-14) as

$$\tilde{\Sigma}_\uparrow^{\mathrm{I}}(\omega) = \pi U^2\theta(-\omega)\theta(-\omega-\omega_{\mathrm{m}})D_\downarrow^0(\omega+\omega_{\mathrm{m}}). \tag{A-26}$$

Since as mentioned above the pole in $D_\downarrow^0(\omega)$ lies above $\omega = 0$, the only contribution to $\tilde{\Sigma}_\uparrow^{\mathrm{I}}(\omega)$ is from the band part of $D_\downarrow^0(\omega)$, and hence from equation (A-17) with $D_\downarrow^0(\omega+\omega_{\mathrm{m}}) \sim [4\Delta_0/\pi U^2]\theta(|\tilde{\omega}+\tilde{\omega}_{\mathrm{m}}|-\tilde{\delta})$, the leading asymptotic behaviour of $\tilde{\Sigma}_\uparrow^{\mathrm{I}}(\omega)$ for $\tilde{U} \gg 1$ is simply

$$\tilde{\Sigma}_\uparrow^{\mathrm{I}}(\omega) \overset{\tilde{U}\gg 1}{\sim} 4\theta\Big[-(\tilde{\omega}+\tilde{\delta}+1)\Big]\Delta_0. \tag{A-27}$$

Equation (A-25) and equation (A-27) are the central equations for the dynamical self-energies employed in Section 5.

References

1. P.W. Anderson, Phys. Rev. **124**, 41 (1961)
2. A.C. Hewson, *The Kondo Problem to Heavy Fermions* (Cambridge University Press, Cambridge, 1993)
3. L.P. Kouwenhoven et al., in *Mesoscopic Electron Trans*port, edited by L.L. Sohn (Kluwer, Dordrecht, 1997)
4. O. Sakai, Y. Shimitzu, H. Shiba, K. Satori, J. Phys. Soc. Jpn. **62**, 3181 (1993)
5. T. Yoshioka, Y. Ohashi, J. Phys. Soc. Jpn. **69**, 1812 (1999)
6. J. Bauer, A. Oguri, A.C. Hewson, J. Phys.: Condens. Matter **19**, 486211 (2007)
7. A.V. Balatsky, I. Vekhter, J.X. Zhu, Rev. Mod. Phys. **78**, 373 (2006)
8. T. Saso, J. Phys. Soc. Jpn. **61**, 3439 (1992)
9. J. Ogura, T. Saso, J. Phys. Soc. Jpn. **62**, 4364 (1993)
10. K. Takegahara, Y. Shimitzu, O. Sakai, J. Phys. Soc. Jpn. **61**, 3443 (1992)
11. K. Chen, C. Jayaprakash, Phys. Rev. B **57**, 5225 (1998)
12. C.C. Yu, M. Guerrero, Phys. Rev. B **54**, 8556 (1996)
13. M.R. Galpin, D.E. Logan, submitted for publication
14. D.E. Logan, M.P. Eastwood, M.A. Tusch, J. Phys.: Condens. Matter **10**, 2673 (1998)
15. M.T. Glossop, D.E. Logan, J. Phys.: Condens. Matter **14**, 6737 (2002)
16. N.L. Dickens, D.E. Logan, J. Phys.: Condens. Matter **13**, 4505 (2001)
17. D.E. Logan, M.T. Glossop, J. Phys.: Condens. Matter **12**, 985 (2000)
18. M.T. Glossop, D.E. Logan, J. Phys.: Condens. Matter **15**, 7519 (2003)
19. R. Bulla, M.T. Glossop, D.E. Logan, Th. Pruschke, J. Phys.: Condens. Matter **12**, 4899 (2000)
20. M.T. Glossop, G.E. Jones, D.E. Logan, J. Phys. Chem. B **109**, 6564 (2005)
21. N.S. Vidhyadhiraja, V.E. Smith, D.E. Logan, H.R. Krishnamurthy, J. Phys.: Condens. Matter **15**, 4045 (2003)
22. D.E. Logan, N.S. Vidhyadhiraja, J. Phys.: Condens. Matter **17**, 2935 (2005)
23. N.S. Vidhyadhiraja, D.E. Logan, J. Phys.: Condens. Matter **17**, 2959 (2005)
24. M.R. Galpin, D.E. Logan, J. Phys.: Condens. Matter **17**, 6959 (2005)
25. P.W. Anderson, G. Yuval, D.R. Hamann, Phys. Rev. **1**, 4464 (1970)